Leaf hydraulics II: Vascularized tissues[☆]

Fulton E. Rockwell[a,*], N. Michele Holbrook[b], Abraham Stroock[a]

[a] *School of Chemical and Biomolecular Engineering, Cornell University, Ithaca, NY 14853, USA.*
[b] *Organismal and Evolutionary Biology, Harvard University, Cambridge, MA 02138, USA.*

Abstract

Current models of leaf hydration employ an Ohm's law analogy of the leaf as an ideal capacitor, neglecting the resistance to flow between cells, or treat the leaf as a plane sheet with a source of water at fixed potential filling the midplane, neglecting the discrete placement of veins as well as their resistance. We develop a model of leaf hydration that considers the average conductance of the vascular network to a representative areole (region bounded by the vascular network), and represents the volume of tissue within the areole as a poroelastic composite of cells and air spaces. Solutions to the 3D flow problem are found by numerical simulation, and these results are then compared to 1D models with exact solutions for a range of leaf geometries, based on a survey of temperate woody plants. We then show that the hydration times given by these solutions are well approximated by a sum of the ideal capacitor and plane sheet times, representing the time for transport through the vasculature and tissue respectively. We then develop scaling factors relating this approximate solution to the 3D model, and examine the dependence of these scaling factors on leaf geometry. Finally, we apply a similar strategy to reduce the dimensions of the steady state problem, in the context of peristomatal transpiration, and consider the relation of transpirational gradients to equilibrium leaf water potential measurements.

Keywords: Poroelasticity, leaf hydraulics, rehydration kinetics, plant water relations

1. Introduction

1.1. Characterizing the hydraulic constraints on leaves

As plants open their stomata to allow the inward flux of CO_2, the chemical potential of liquid phase water at the evaporating sites falls until, in steady state, the resulting flux of liquid water into the leaf balances the flux of water vapor from the stomata. Thus, measures of the hydraulic efficiency of the liquid flow correlate with maximum stomatal aperture, and therefore carbon gain (Boyce et al., 2009; Brodribb et al., 2007). Yet, the extent to which this hydraulic efficiency is determined by the transport properties of the cells and airspaces that make up the tissue between the leaf veins and the stomata, or depends directly on the characteristics of the vascular system itself, remains uncertain. While vein density has been shown to correlate with various measures of leaf water transport efficiency at broad phylogenetic scales (Brodribb et al., 2007, 2010), the relationship is likely not strictly causal. In angiosperms, the dominant resistance to liquid flow in a leaf is believed to reside downstream of the veins, in the tissue outside the vasculature (Cochard et al., 2004; Sack et al., 2004; Brodribb et al., 2010). Vascular conductance per unit leaf area may then simply scale with the resistance of the tissue path. Yet while the partitioning of leaf transport properties between vasculature and tissue may be central to understanding hydraulic limits on leaf level productivity, current practice in plant physiology lumps vascular and tissue properties into a single whole-leaf conductance, K_{leaf} (Sack et al., 2002).

A major obstacle to partitioning 'whole-leaf' transport properties between vasculature and tissue is a lack of models that describe these different pathways in terms of experimentally available, physically well-defined parameters. For example, whole-leaf hydraulic conductances (K_{leaf}) are often defined as the proportionality between an observed flux and the difference in water potential between the leaf and a source, typically a reservoir (lab) or branch (in situ) of known water potential (Scoffoni et al., 2008; Brodribb and Holbrook, 2006). While seen as offering the advantage of defining a conductance under transpiring conditions, the water potential of the leaf is in fact measured under non-transpiring conditions, typically in the pressure chamber. This leads to ambiguity in the description of the driving force for the observed flux, as the pressure chamber reports the volume and capacitance weighted average potential of the tissue, once the gradients induced by transpiration have collapsed, and not the potential at the sites of evaporation within the leaf that we seek (Boyer, 1985; Sack et al., 2002).

Other characterizations of K_{leaf} have their own limitations. In high pressure flow methods, the driving force is well defined, but the flow path measured is unknown (Tyree and Cheung, 1977), a problem that applies equally to methods where a reduction in the pressure in the liquid phase at the air water interfaces inside the leaf blade is imposed by means of a vacuum pump. Consequently, it is not possible to directly relate conductances defined by such methods to material properties of the

[☆] This work was supported by the National Science Foundation (award no. DBI 1103664)(F.E.R.), and the Air Force Office of Sponsored Research (award no. FA9550-09-1-0188) (A.S. and N.M.H.).

[*] Corresponding author. Tel.: +1 914 456 1917.
Email address: fulton.rockwell@gmail.com (Fulton E. Rockwell)

leaf. Indeed, we do not even know how to compare hydraulic conductances defined by evaporative methods to high pressure flow methods (Sack et al., 2002). The fact that K_{leaf} is not in general a physically well-defined quantity may also underlie its apparent response to exogenous environmental factors that alter the flux (Rockwell et al., 2011).

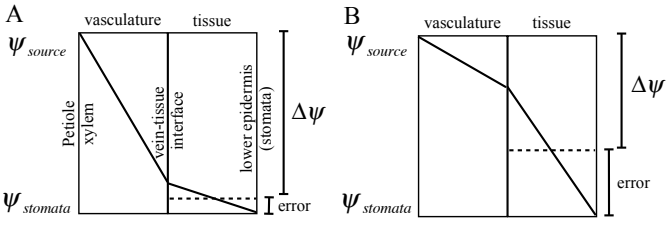

Figure 1: 1D steady-state model a leaf as vascular and tissue resistance in series, with the liquid flux driven by the potential difference $\psi_{source}-\psi_{stomata}$ (Brodribb et al., 2010). In practice, the flux is directly observed, and the $\Delta\psi$ driving that flux is taken as the difference between source and whole leaf potential as measured by the pressure chamber (dotted line). As the latter reports the average potential of the tissue, unless vascular resistance dominates (**A**) the error may be large (**B**).

Nevertheless, some effort has been made to separate the vascular and tissue components conceptually with respect to steady state evaporative methods, and account for the effect of vein spacing. Brodribb et al. (2010) propose a 1D model relating whole leaf conductance to leaf structure by invoking an electrical analogy, decomposing the K_{leaf} of a transpiring leaf into a vascular and mesophyll conductance in series, where the mesophyll conductance is defined as the distance D_m from a vein to the furthest evaporating site divided by the hydraulic conductivity of the mesophyll cells. The model is then made concrete by assuming that all evaporation is peristomatal, and defining D_m as the hypotenuse of a right triangle formed by the distance from a vein to the epidermis, and half the inter-vein distance. This D_m is taken as the effective length of transport through the tissue that incorporates the effect of vein spacing. Yet K_{leaf} is still defined experimentally as the proportionality between the flux and the difference between source potential and average potential of the tissue reported by the pressure chamber. So defined, K_{leaf} contains an implicit assumption of negligible gradients in the tissue during transpiration, one required if the average potential of the tissue is to converge with the difference in potential between the lower epidermis and source (Figure 1). Furthermore, we do not know how faithfully the definition of D_m maps the 1D series model to what is at least a 2D problem in the case of parallel veins, and a 3D problem for reticulate veins.

Alternatively, progress in unravelling the hydraulics constraints on leaves may be made by characterizing tissue hydraulic properties through isothermal rehydration experiments (i.e., non-transpiring conditions), and then modeling the non-isothermal competition between vapor and liquid transport in the leaf, to satisfy an observed transpirational flux. This approach avoids the uncertainties regarding driving force or path length that complicate both the evaporative and high pressure flow methods. For rehydration experiments, the difference in initial and final water potentials is well defined if the measurements are made at equilibrium (Boyer, 1995). In addition, the location of the 'sinks' for water uptake are the same as for a pressure-volume curve, providing the relationship between changes in potential and changes in water content during the transient. The only uncertainty remaining for the isothermal transient analysis is the form of an appropriate model by which potential differences and time are related, one that captures the effect of a tissue hydrating through an embedded vascular network. This uncertainty we attempt to address here.

1.2. Current models of leaf hydration

Two approaches to modeling transient leaf hydration can be found in the literature. The first approach adopts a discrete ohms law analogy (Brodribb and Holbrook, 2004), that treats the leaf as a vascular 'resistor' in series with a capacitor, the leaf tissue, which stores charge (water) but has negligible internal resistance itself (Horowitz and Hill, 1989). As we will show, this approach conforms to the assumption of a dominant vascular resistance. The second approach is based on a continuum description that smooths discrete cellular permeabilities into tissue conductivities. Here the capacity for water storage is *distributed* throughout a resistive medium, arriving at a mathematical form analogous to the one-dimensional heat equation (Philip, 1958a). This form has been employed to describe volume uptake and water potential relaxation in leaf tissues (Boyer, 1968, 1969), neglecting vascular resistance by assuming a fixed, continuous source potential at the leaf midplane. Here we show that both of these models can be derived as the limiting cases of a more general model describing transient flow through a rigid network in series with an elastic tissue.

We have previously considered the transport properties of leaf tissue as a composite of protoplasts, cell wall, and air space (**?**). We now attempt to account for the leaf vasculature in terms of an average conductance from a source at the petiole to any point within the leaf along the vein-tissue interface. The analysis is complicated by the fact that the veins occupy discrete locations in the vascular plane in a leaf, rather than forming a continuous plane of supply, resulting in a 3D 'partially-active' boundary condition problem that necessitates numerical simulation to find a solution. By comparing the 3D numerical simulations to the general form of a 1D analytic solution, we evaluate the utility of the assumption of a continuous plane of vascular supply as a way of arriving at a 1D form of the transient hydration problem. We also evaluate the use of the 'effective length' of Brodribb et al. (2010), D_m, to account for the discrete placement of the veins. Finally, we seek scaling factors that reduce the 3D problem to an equivalent 1D form, and examine the relationship between these factors and leaf geometry through regression analysis.

2. Model development

2.1. Representation of the vascular network

During a rehydration experiment, water flows from a source reservoir at constant potential, through the petiole and leaf

Table 1: Symbol definitions

Quantity	Symbol	Units
Leaf half-thickness	L	m
Vein to lower epidermis	l_e	m
Vascular xylem half width	a	m
Effective length	D_m	m
Intervein distance	w	m
Area	A	m^2
Volume	V	m^3
Uptake (cumulative flow)	Q	mol
Molecular flux	J	$mol\ m^{-2}\ s^{-1}$
Water potential	ψ	Pa
Characteristic time	τ	s
Poroelastic Diffusivity	κ	$m^2\ s^{-1}$
Hydraulic capacity	c	$mol\ m^{-3}\ Pa^{-1}$
Leaf capacitance	c_A	$mol\ m^{-2}\ Pa^{-1}$
Vascular conductance	h	$mol\ m^{-2}\ Pa^{-1}\ s^{-1}$
Hydraulic conductivity	k	$mol\ m^{-1}\ Pa^{-1}\ s^{-1}$
Leaf hydraulic conductance	K_{leaf}	$mol\ m^{-2}\ Pa^{-1}\ s^{-1}$

Table 2: Dimensionless symbols

Dimensionless Quantities	Symbols	
Potential	Ψ	
Time	T	
Uptake	Φ	
Biot number	$\mathcal{B}$	
Subscripts & Superscripts	**Symbols**	
Leaf tissue	ℓ	
Reservoir	r	
Initial state	o	
Final state	f	
Leaf area basis	A	
Vein area basis	V	
Vein to epidermis	e	
Hypotenuse model	$\triangle$	
3D to 1D Scaling Factors	**Symbols**	**Equations**
Transient hydration	$\xi,\ \eta$	53-58
Steady state flux	$\varsigma,\ \zeta,\ \epsilon$	59-63
Leaf to epidermal potential	$\phi,\ \omega$	65, 66
Vasc. volume correction	γ	17

xylem, and into the tissue that then changes in water content. Boyer (1968, 1969) idealized the hydration of a leaf as a one dimensional flow from the vascularized midplane, regarded as a continuous source of water at a fixed potential, toward the upper and lower epidermis, which hydrate in parallel. This approach involves two related assumptions. First, that the network of veins is sufficiently conductive relative to the tissue that vascular potential, at every point in the network, sits very close to the potential of the external reservoir. Second, that the veins are sufficiently close together that lateral gradients in the tissue between the veins are small, and the flow is nearly unidirectional (one dimensional) through the leaf thickness. To the extent that these assumptions are not met, this model's estimate of the tissue conductivity will be lower than the true value, as the resistance that derives both from flow through the vasculature and the spacing between veins will be assigned to the tissue.

Here we first relax the assumption of negligible vascular resistance. For the leaves of many plants, we expect that the axial resistance of the xylem is small (but not negligible) relative to the radial resistance through the tissue (Cochard et al., 2004; Ye et al., 2008). If the leakage to the tissue is concentrated in the highest (smallest) vein orders, then we can consider each areole as hydrating in parallel, and neglect the presumably small variations in the axial conductance *to* each areole. Similarly, if the total vascular pressure drop is large relative to the variation *within* the vasculature of an areole, we can then approximate the xylem network as providing a single average vascular conductance, h_V, to every point along the vein-tissue interface.

As the veins inhabit discrete locations within the vascular plane, rather than filling it to provide a continuous boundary, they constitute a 'partially active' boundary condition, as occurs in chemical engineering problems where one or more of the boundaries of a domain of interest is composed of a patchwork of catalytic and inert surfaces (Dudukovic and Mills, 1985). Such problems in 3D do not admit an analytic solution. Therefore, to relax the second assumption of one dimensionality, we employ a numerical analysis of the full 3D problem. We then study how the 3D problem may be mapped to a 1D, continuous boundary value problem, for which we can find a closed form mathematical solution useful for interpreting hydration experiments.

2.2. Specification of the domain of interest

We consider a leaf with reticulate venation, in which the highest vein orders demarcate approximately square domains of tissues (areoles), with a width and depth $2w$, and a thickness from lower to upper epidermal surfaces $2L$ (Figure 2 A). As the gradients in potential will be symmetrical about the center of the vein, and the mid-plane between veins, we consider a domain of 1/4 of an areole, or $w \times w \times 2L$. The vascular plane (vp) is located at the transition between spongy and palisade parenchyma, a distance l_e from the lower epidermis, such that vp marks the plane of the lower surface of a vein's xylem. The distance to the lower epidermis l_e, vp, and the half thickness of the leaf L are related by,

$$l_e = 2L \cdot (1 - vp). \tag{1}$$

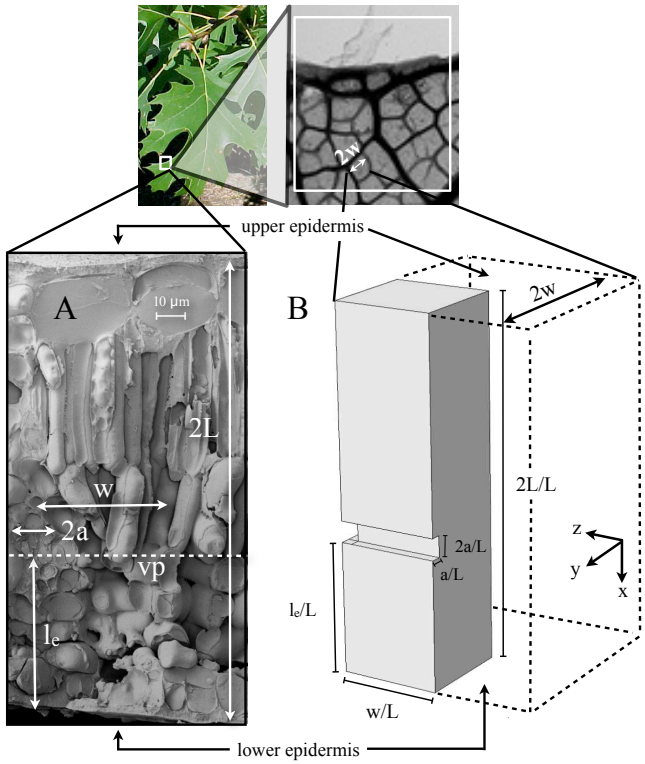

Figure 2: Geometry of a *Quercus rubra* leaf. **A**: Cryo-SEM cross section through the leaf thickness $2L$, showing vein width $2a$, areole half-width w, plane of vasculature vp, and distance to lower epidermis l_e. **B**: Normalized geometry of a representative quarter areole (grey); the full areole is demarcated by dotted lines, and defined as a domain of tissue $2w \times 2w$ bounded by the vascular network. Water enters across the surfaces of the cut-out vein volume.

In the cross section of a vein (middle left side of Figure 2 A), the width and height of the xylem in the vascular bundle is defined as $2a$, such that the xylem in a bundle forms a square with a total perimeter $8a$. To simplify the boundary conditions, we approximate the xylem filled part of the vein as square, filling an L shaped region in the quarter areole with a total surface area $8 \cdot (a \times w) - 6a^2$. It is on the xylem boundary, rather than the boundary of the vascular bundle inclusive of the phloem, that we locate the vein-tissue interface and the transition from vascular to tissue transport. To describe the effect of transport though the vasculature on the availability of water at the vein-tissue interface, we define h_v as the effective conductance of the vascular network to the vein-tissue interface within a representative areole. The principal source of estimates of h_V are vein cutting experiments, which define a conductance h_A based on the flux and pressure drop between the petiole and the cut-vein order that is then normalized to the leaf area (Sack et al., 2004). An estimate of h_V then follows from re-normalizing to the vein surface area, or

$$h_V = h_A \left(\frac{w^2}{8aw - 6a^2} \right) \tag{2}$$

The interior of the domain we regard filled by a homogenous, isotropic tissue. The description of leaf tissue as a homogenous, isotropic media composed of protoplasts, cell walls, and airspace, has been addressed previously (**?**). Briefly, for deformations of a few percent, as occur in rehydration experiments, we neglect the changes in dimensions and between-cell mechanical interactions that accompany water uptake. The resulting equation governing transient hydration has the form of the heat equation, with a hydraulic capacity, c_ℓ, the moles of water stored per unit nominal volume per unit potential, playing a role similar to that of a heat capacity.

The hydraulic capacity of leaf tissue is in practice defined from the linearized slope of a leaf pressure-volume curve, normalized to the leaf blade volume. As we have excluded the vascular volume from our domain of interest, the hydraulic capacity of the 3D domain must be renormalized from the 'full' volume $2L \cdot w^2$ to the domain volume, leading to

$$c_\ell^{3D} \equiv c_\ell \left(1 - \frac{a^2}{w^2} \left(\frac{2w - a}{L} \right) \right)^{-1}. \tag{3}$$

Here we introduce the superscript 3D to keep track of parameters defined specifically in relation to the 3D domain. The ratio of the hydraulic conductivity of the tissue to hydraulic capacity then forms a poroelastic diffusivity κ_ℓ, which together with the length L of the tissue over which transport occurs defines τ, the characteristic time scale for the propagation of potential or volume change in the tissue,

$$\kappa_\ell^{3D} \equiv \frac{k_\ell}{c_\ell^{3D}}, \qquad \tau^{3D} \equiv \frac{L^2}{\kappa_\ell^{3D}}. \tag{4}$$

The intrinsic behavior of our domain of tissue during a transient between two hydration states is then completely characterized by the time τ^{3D}.

2.3. Non-dimensionalization of the 3D transient problem

We will follow the standard practice of transforming the equations we are studying by substituting non-dimensional variables (Deen, 1998; Bridgman, 1922). One advantage of this approach is that is makes the mathematical structure of a problem and its solution clearer. For example, non-dimensionalization organizes the parameters in a problem into one or more dimensionless groups upon which the solution then depends: the value of a particular parameter only really matters in relation to the others with which it is grouped. To rescale the physical dimensions, we adopt the half thickness L as the characteristic length of the problem, and introduce new spatial variables ($X = x/L,\ Y = y/L,\ Z = z/L$). The resulting domain is shown in Figure 2 B. The potential is normalized by,

$$\Psi = \frac{\psi - \psi_r}{\psi_o - \psi_r}, \tag{5}$$

where ψ_r is the potential of the reservoir supplying the petiole, and ψ_o is the initial potential of the leaf. The epidermal surfaces located at ($X = 0, 2$) constitute insulated (no-flux) boundaries as long as the stomata are closed. The faces of the domain shared with the neighboring areoles, hydrating in parallel, are also no-flux boundaries by symmetry. Thus, everywhere on the domain surface σ, except the vascular surfaces σ_V, the flux across the surface is zero,

$$\text{On } \sigma \neq \sigma_V, \qquad \vec{n} \cdot \nabla\Psi = 0, \tag{6}$$

where $\vec{n}$ is the normal vector to the domain surface.

On the vascular surfaces, the flux into the tissue must be equal to the flux from the reservoir to the vascular surface. Labeling the vascular surfaces according to their normal vectors (e.g., the vascular surface lying in the YZ plane is σ_x), the rescaled boundary conditions on the vascular surfaces become,

$$\text{On } \sigma_{Vx}: \ -k_\ell \frac{\partial\psi}{\partial x} = h_V(\psi_r - \psi) \rightarrow -\frac{\partial\Psi}{\partial X} + \frac{h_V L}{k_\ell}\Psi = 0, \tag{7}$$

$$\text{On } \sigma_{Vy}: \ -k_\ell \frac{\partial\psi}{\partial y} = h_V(\psi_r - \psi) \rightarrow -\frac{\partial\Psi}{\partial Y} + \frac{h_V L}{k_\ell}\Psi = 0, \tag{8}$$

$$\text{On } \sigma_{Vz}: \ -k_\ell \frac{\partial\psi}{\partial z} = h_V(\psi_r - \psi) \rightarrow -\frac{\partial\Psi}{\partial Z} + \frac{h_V L}{k_\ell}\Psi = 0. \tag{9}$$

The non-dimensional groups scaling the potential at the vascular boundary represent the ratios of vascular to tissue conductance over the lengths of the domain along the coordinate axes. Similar ratios of parameters arise in the analysis of many heat transfer problems, as for example the ratio of the heat conductance away from a body to the thermal conductivity of the body over its characteristic size. This combination of a conductance, length and a conductivity arises often enough in heat transfer that it is termed a Biot number (Lienhard IV and Lienhard V, 2006), and given the symbol $\mathcal{B}$. Here we will borrow that convention, and define $\mathcal{B}^{3D} = h_V L/k_\ell$. Within the domain, the equation governing the potential field during the transient has the form of the heat equation (Philip, 1958b; **?**), and after the change of variables becomes,

$$\frac{\partial\Psi}{\partial t} = \kappa_\ell^{3D}\left(\frac{\partial^2\Psi}{L^2\partial X^2} + \frac{\partial^2\Psi}{L^2\partial Y^2} + \frac{\partial^2\Psi}{L^2\partial Z^2}\right), \tag{10}$$

$$\text{I.C.}: \ \Psi(X, Y, Z, t \leq 0) = 1, \tag{11}$$

subject to the above boundary conditions. We next define a non-dimensional time variable $T^{3D} = t/\tau^{3D}$, such that,

$$\frac{\partial\Psi}{\partial T^{3D}} = \left(\frac{\partial^2\Psi}{\partial X^2} + \frac{\partial^2\Psi}{\partial Y^2} + \frac{\partial^2\Psi}{\partial Z^2}\right), \tag{12}$$

$$\text{I.C.}: \ \Psi(X, Y, Z, T^{3D} \leq 0) = 1. \tag{13}$$

This completes the specification of the 3D problem. Since we have normalized time to the time scale of the tissue in the domain, the non-dimensional 3D solution varies only as a function of the ratio of vascular conductance to transport through the tissue ($\mathcal{B}^{3D}$), which enters through the boundary conditions, the length ratio w/L that enters through the geometry of the domain, and a/L and vp which enter through the geometry of the vascular-tissue interface. The numerical solutions can then be tabulated as a function of $\mathcal{B}^{3D}, w/L, a/L$, and vp.

2.4. Estimating k_ℓ^{3D} from transient experiments

As in practice plant physiologists are limited to only equilibrium measurements of water potential, what we want to know is the average potential within the the domain at each point in time, which is to say the uniform potential the entire domain ultimately goes to if it is allowed to come to internal equilibrium after t seconds of hydration. We therefore average the numerical solution for the potential field across the domain at each time step, to arrive at a solution for the equilibrium potential of the leaf (a single value) as a function of the time variable T^{3D}, or $\Psi(T^{3D})$. We next define the non-dimensional halftime $T_{1/2}^{3D}$ as the value of T^{3D} at which $\Psi = 0.5$, when the initial potential has relaxed halfway toward its ultimate value, equal to that of the source. For any particular geometry as defined by $w/L, a/L, vp$, the numerical value of $T_{1/2}^{3D}$ will vary, as indeed the full solution does, as a function of $\mathcal{B}^{3D}$. However, as $\mathcal{B}^{3D}$ itself depends on the unknown value of k_ℓ, estimating k_ℓ involves iteration. For each value of $T_{1/2}^{3D}$, an estimate of k_ℓ follows from an experimental observation of the half-time for volume uptake or potential relaxation, $t_{1/2}$, and the identity,

$$\frac{c_\ell^{3D} L^2}{k_\ell^{3D}} \equiv \tau^{3D} \equiv \frac{t_{1/2}}{T_{1/2}^{3D}}. \tag{14}$$

From all of these values of k_ℓ^{3D}, each associated with a particular value of $\mathcal{B}^{3D}$, the value that satisfies the definition of the Biot number,

$$k_\ell^{3D} = \frac{h_v L}{\mathcal{B}^{3D}}, \tag{15}$$

provides the desired estimate of the hydraulic conductivity of an experimental leaf's tissue. In summary, this procedure characterizes k_ℓ for a given leaf, given estimates of h_A, c_ℓ, L, w, a, vp, and $t_{1/2}$.

2.5. Survey of leaf geometrical parameters

To study the behavior of the numerical solution to the 3D problem as a function of leaf geometry, we calculated w/L, a/L, and the location of the vascular plane vp (taken as the transition from palisade to spongy mesophyll), for 23 temperate woody species. For *Quercus rubra*, we estimated these parameters based on fresh microtome sections viewed at 200x (n=5). For the 22 other taxa, published data included bundle sheath cell diameter, but not the minor vein xylem width $2a$. To estimate the latter, we noted that, based on paradermal sections for these leaves (Wylie, 1939), as well as two other studies (Dengler and MacKay, 1975; Russin and Evert, 1984), and *Quercus rubra* (this study), the width of the xylem in the smallest veins typically is on the order of one bundle sheath cell diameter, such that $2a = D_{bsc}$. For the survey data lacking direct measurements of minor vein widths, adopting this rule for a resulted in a mean minor vein half-width of 5.9 μm, with a range of 4 to 8. These estimates appear to be in accord with the typical minor vein radius of 6 μm for dicotyledons reported by Armacost (1944), as cited by Sack et al. (2004). Our xylem source region, the cut out volume in Figure 2 A, $2a$ high and $2a$ wide on the adaxial side of the vascular plane, is therefore equivalent to an interface with three bundle sheath parenchyma on the top and sides of the xylem, plus an interface with the phloem side of the vein $2a$ long. In this accounting, the phloem is considered part of the tissue.

It should be noted that in the steady state analyses to follow we will assume these leaves have open stomata only on the lower epidermal surface, yet at least *Populus deltoides* is known by us to have stomata on both surfaces. Nevertheless, its inclusion in the analysis is not unreasonable, insofar as under conditions of high evaporative demand such leaves may preferentially shut stomata on the upper surface and so be functionally hypostomatous (Foster and Smith, 1986). For this species, the results should be viewed as limited to those conditions.

2.6. Basis for transient 3D and 1D model comparisons

To find a 1D representation, we construct a homogenous boundary condition by assuming a continuous vascular plane (CVP) at the midpoint through the leaf thickness, with a conductance to each of the upper and lower halves of the leaf defined as $h = h_A/2$ (Figure 3). To compare such a 1D model to the 3D model above, we expect we can again can express the solution in terms of a non-dimensional halftime, $T_{1/2}^{1D}$ and a characteristic time τ^{1D}, as

$$t_{1/2} = T_{1/2}^{1D} \cdot \tau^{1D}, \quad \tau^{1D} = \frac{c_\ell^{1D} L^2}{k_\ell^{1D}}, \quad \mathcal{B}^{1D} = \frac{h}{h_V}\mathcal{B}^{3D}. \tag{16}$$

By definition, if the solutions are equivalent the ratio of their halftimes $t_{1/2}$ must be one. We now use this fact to develop a criterion for how well an estimate of tissue conductivity, based on the 1D model, will conform to the tissue conductivity fitted by the 3D model. The ratio of the halftimes leads to an expression for the ratio of the tissue conductivities predicted by the 1D and 3D models that can be evaluated in terms of the dimensionless halftimes;

$$1 = \frac{T_{1/2}^{1D} \cdot \tau^{1D}}{T_{1/2}^{3D} \cdot \tau^{3D}} = \frac{T_{1/2}^{1D}}{T_{1/2}^{3D}} \frac{c_\ell^{1D}}{c_\ell^{3D}} \frac{k_\ell^{3D}}{k_\ell^{1D}},$$
$$\frac{k_\ell^{1D}}{k_\ell^{3D}} = \frac{T_{1/2}^{1D}}{T_{1/2}^{3D}}\gamma, \qquad \gamma = 1 - \frac{a^2}{w^2}\left(\frac{2w-a}{L}\right). \tag{17}$$

The factor γ is required to account for the small difference in the tissue volume to which c is referenced in the two models. With (17), and the relationship between $\mathcal{B}^{3D}$ and $\mathcal{B}^{1D}$ in (16), we have arrived at a test of the ability of the 1D model to capture the behavior of the full 3D problem. Equation (17) says that for the 1D model to provide an estimate of tissue hydraulic conductivity in tolerable agreement with the 3D model, we require that $\gamma T_{1/2}^{1D}/T_{1/2}^{3D} \approx 1$. To find $T_{1/2}^{1D}$ as a function of $\mathcal{B}^{1D}$, we need to solve the 1D problem, which we turn to below.

2.7. Analytic solutions to the 1D transient problem

While in the 3D problem statement the location of the vascular plane was a variable independent of the leaf thickness, for the 1D problem we consider flow toward either epidermis through the average thickness, equal to half the leaf thickness. Centering the coordinate system on the mid-plane, we focus on a 1D domain that spans a distance 0 to L in x, which hydrates in parallel with the domain from 0 to $-L$ (Figure 3). The evolution of the water potential field is then governed by,

$$\frac{\partial \psi}{\partial t} = \kappa_\ell^{1D}\frac{\partial^2 \psi}{\partial x^2}, \qquad \kappa_\ell^{1D} \equiv \frac{k_\ell^{1D}}{c_\ell^{1D}}. \tag{18}$$

In the case the stomata are closed, there is no flux across the epidermis at L,

$$\left.\frac{\partial \psi}{\partial x}\right|_{x=L} = 0 \qquad \text{for all } t, \tag{19}$$

while at the mid plane at $x = 0$, the flux into one half-thickness of the leaf is equal to half the flux from the reservoir to the midplane,

$$-k_\ell^{1D}\left.\frac{\partial \psi}{\partial x}\right|_{x=0} = h\left(\psi_r - \psi\left(x = 0, t > 0\right)\right), \tag{20}$$

where again, $h = h_A/2$. Re-scaling the variables according to,

$$X = \frac{x}{L} \qquad T^{1D} = \frac{t}{\tau^{1D}} \qquad \Psi = \frac{\psi - \psi_r}{\psi_o - \psi_r}, \tag{21}$$

we define the characteristic time τ^{1D} with the hydraulic capacity as it is generally defined (i.e., normalized to the entire leaf blade volume),

$$\tau^{1D} = \frac{c_\ell^{1D} L^2}{k_\ell^{1D}}, \tag{22}$$

to arrive at the dimensionless form of the 1D problem,

$$\frac{\partial \Psi}{\partial T^{1D}} = \frac{\partial^2 \Psi}{\partial X^2}. \tag{23}$$

The initial and boundary conditions are transformed to

Table 3: Survey of temperate deciduous leaf geometry with the resulting 3D to 1D scaling factors from the numerical simulations

Source: Wylie (1939), *except as noted.*	D_{bsc} μm	L μm	w μm	a μm	vp -	ξ -	η -	ζ -	ϵ -	ϕ -	ω -
Ulmus americana	12	83.7	40.5	6	0.65	1.261	1.046	0.113	1.057	0.759	-0.254
Ailanthus glandulosa	8.5	86.15	34.75	4.25	0.6	1.304	1.044	0.092	1.032	0.736	-0.255
Syringa vulgaris	14.3	156.5	59.7	7.15	0.64	1.316	1.040	0.099	1.029	0.751	-0.246
Populus deltoides[2]	14	110	55.6	7	0.5	1.353	1.025	0.090	1.041	0.695	-0.266
Platanus occidentalis	10.6	82.2	42.3	5.3	0.63	1.378	1.036	0.125	1.041	0.738	-0.241
Quercus velutina	12	92.3	49.45	6	0.57	1.398	1.026	0.112	1.040	0.712	-0.251
Rus glabra	11.3	90.3	46.9	5.65	0.65	1.420	1.040	0.136	1.038	0.740	-0.232
Robinia pseudo-acacia	8	58.6	34	4	0.64	1.475	1.035	0.148	1.039	0.729	-0.228
Quercus rubra[3]	12.1	102.4	57.4	6	0.64	1.532	1.050	0.151	1.030	0.721	-0.219
Fagus grandifolia[1]	10.5	80	55	5.4	0.5	1.676	1.023	0.138	1.030	0.662	-0.229
Vitis vulpina	16.6	75	70.2	8.3	0.54	1.706	1.025	0.179	1.058	0.664	-0.228
Quercus macrocarpa	7.8	68.1	44.9	3.95	0.61	1.769	1.023	0.182	1.023	0.686	-0.199
Tilia americana	13	56.5	56.5	6.5	0.49	1.797	1.045	0.176	1.058	0.641	-0.230
Malus ionesis	11	70.6	60.9	5.5	0.58	1.925	1.023	0.213	1.032	0.661	-0.197
Catalpa speciosa	14	71.5	79	7	0.5	2.196	1.023	0.232	1.037	0.618	-0.195
Parthenocissus quinquefolia	15.4	82.8	90.2	7.7	0.49	2.230	1.023	0.229	1.034	0.613	-0.194
Cercis canadensis	12	61	70.5	6	0.49	2.309	1.024	0.242	1.035	0.607	-0.191
Acer saccharinum	10.2	43.4	76.5	5.1	0.56	3.401	1.044	0.483	1.033	0.541	-0.131
Aristolochia durior	11	47.5	86	5.5	0.51	3.584	1.031	0.451	1.031	0.526	-0.135

[1]Dengler (1975), [2]Russin (1984), [3]this study.

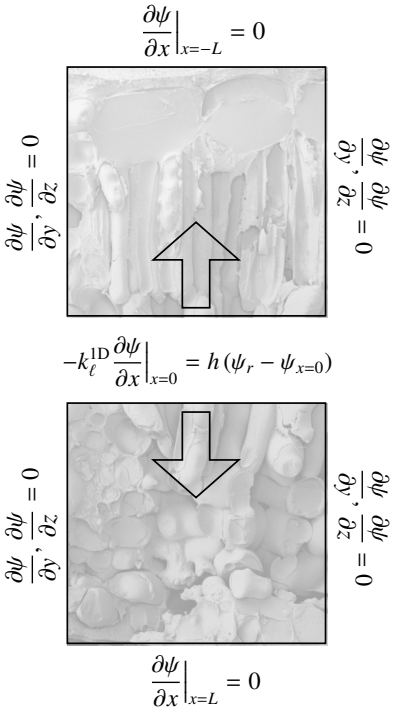

Figure 3: 1D Continuous Vascular Plane (CVP) model of leaf hydration. The vasculature is represented as an effective conductance h independently supplying both domains, above and below the mid-plane of the leaf at $x = 0$, such that hydration of the tissues towards the upper and lower surfaces (epidermi) at $x = -L, L$ occurs in parallel.

$$\Psi(X, T^{1D} \leq 0) = 1, \tag{24}$$

$$\frac{\partial\Psi}{\partial X}\Big|_{X=1} = 0, \tag{25}$$

$$-\frac{\partial\Psi}{\partial X}\Big|_{X=0} + \frac{hL}{k_\ell^{1D}}\Psi\left(X = 0, T^{1D} > 0\right) = 0. \tag{26}$$

For the 1D model, the Biot number is defined in the second term of (26) as $\mathcal{B}^{1D} = hL/k_\ell^{1D}$. While we have scaled the variables to range from zero to one, and the spatial derivatives to be order one, the magnitude of the Biot number is free to vary, and we can consider the behavior of the mid plane boundary condition in the limit that the Biot number is very large, very small, or about one. A detailed development of the solutions and their approximation is given in Appendix A; the results relevant to the current discussion are given below.

2.7.1. $\mathcal{B}^{1D} \gg 1$

When the Biot number is very large, the water potential of the vascular plane approaches that of the external reservoir, as assumed by Boyer (1968). After a leaf has hydrated for t seconds, and then come to internal equilibrium throughout the tissue, the dominant term and thus approximate solution is given by,

$$\frac{\psi(t) - \psi_r}{\psi_o - \psi_r} \approx \frac{8}{\pi^2}\exp\left(-\frac{\pi^2}{4}\frac{k_\ell}{c_\ell L^2}t\right). \tag{27}$$

The above form is expected to converge with the full solution after an amount of time given by $0.14\,\tau^{1D}$, and the non-dimensional halftime in this limit for comparison with the 3D solution is just $T_{1/2}^{1D} = 0.197$.

2.7.2. $\mathcal{B}^{1D} \ll 1$

In the limit the Biot number is much less than 1, the gradients within the tissue become negligible relative to the gradients through the xylem, justifying a 'lumped-capacity' ohms

law analogy of a resistor (xylem) in series with an ideal capacitor (tissue with zero internal resistance). The solution is then,

$$\Psi(t) = \exp\left(-\frac{h}{c_\ell^{1D} L} t\right). \tag{28}$$

With the change of variables $c_A/(2L) = c_\ell^{1D}$ as the capacitance of the leaf per unit leaf area, and $K_\ell/2 = h$, (28) is the form adopted by (Brodribb and Holbrook, 2004) for quantifying the susceptibility of leaf xylem to cavitation. The non-dimensional halftime is given by,

$$T_{1/2}^{1D} = \frac{0.693}{\mathcal{B}^{1D}}. \tag{29}$$

2.7.3. $\mathcal{B}^{1D} \sim 1$

When the Biot number is between the limiting cases, we solve the full problem (23 to 26), which leads to an expression for the non-dimensional halftime. More simply, in Appendix A we show that the inverted solution for the hydration time can be conveniently approximated as the sum of the time for flow through the vasculature and through the tissue,

$$t(\Psi) = T^{1D}(\mathcal{B}^{1D} \gg 1, \Psi)\tau^{1D} + T^{1D}(\mathcal{B}^{1D} \ll 1, \Psi)\frac{\tau^{1D}}{\mathcal{B}^{1D}}. \tag{30}$$

The non-dimensional halftime is then given by,

$$T_{1/2}^{1D} = 0.197 + \frac{0.693}{\mathcal{B}^{1D}}. \tag{31}$$

The times over which this approximation holds are discussed in the results (3.3).

2.8. Numerical simulation of the 3D steady state problem

To address the question of how well the continuous vascular plane assumption performs in steady state, we first studied the 3D problem for steady flow between the vascular plane at $x = 0$ and the lower epidermis at $x = l_e$, as might occur during transpiration, assuming isothermal transport within the leaf (i.e., if vapor transport due temperature induced gradients in saturated vapor pressure are not important). For the steady state problem, we regard the potential at the lower epidermis ψ_e as the unknown we ultimately wish to solve for, with k_ℓ^{3D} defined by a transient experiment. We then normalize the geometry of the domain according to $X = x/l_e, Y = y/l_e, Z = z/l_e$, such that the lower epidermis is located at $X = 1$. In this setting, a rescaling of the potential into a non-dimensional form that has the desired range from 1 at the source reservoir r to 0 at the lower epidermis e, is given by

$$\Psi = \frac{\psi - \psi_e}{\psi_r - \psi_e}. \tag{32}$$

In the domain, conservation of water molecules in steady state leads to,

$$0 = \left(\frac{\partial^2 \Psi}{\partial X^2} + \frac{\partial^2 \Psi}{\partial Y^2} + \frac{\partial^2 \Psi}{\partial Z^2}\right). \tag{33}$$

With the new definition of Ψ, the boundary conditions at the vascular interface are then,

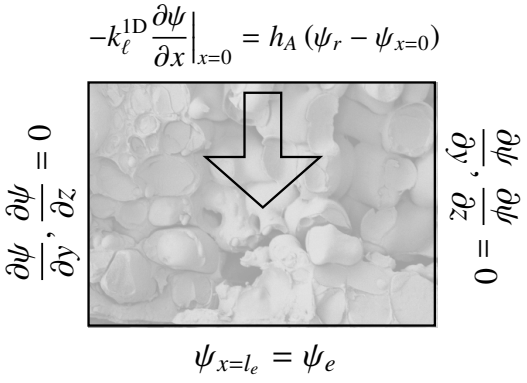

Figure 4: 1D Continuous Vascular Plane (CVP) model for steady flow to the lower epidermis. The vascular conductance h_A spreads the transport capacity of the veins over the entire vascular plane at $x = 0$, a distance l_e from the lower epidermis, with no flow into the portion of the leaf above the plane.

On σ_{vx} :

$$-k_\ell^{3D}\frac{\partial\psi}{\partial x} = h_V(\psi_r - \psi) \rightarrow -\frac{\partial\Psi}{\partial X} + \frac{h_V l_e}{k_\ell^{3D}}(1 - \Psi) = 0, \tag{34}$$

On σ_{vy} :

$$-k_\ell^{3D}\frac{\partial\psi}{\partial y} = h_V(\psi_r - \psi) \rightarrow -\frac{\partial\Psi}{\partial Y} + \frac{h_V l_e}{k_\ell^{3D}}(1 - \Psi) = 0, \tag{35}$$

On σ_{vz} :

$$-k_\ell^{3D}\frac{\partial\psi}{\partial z} = h_V(\psi_r - \psi) \rightarrow -\frac{\partial\Psi}{\partial Z} + \frac{h_V l_e}{k_\ell^{3D}}(1 - \Psi) = 0. \tag{36}$$

Specifying $\Psi = 0$ at the lower epidermis, $(X = 1, Y, Z)$, with the upper epidermis treated as impermeable for the case of a hypostomatous leaf, and a no flux condition by symmetry on all other surfaces as before, completes the 3D problem statement.

We should also note that the form of the Biot number for the steady state problem differs from that of the transient, due to a change in the characteristic length from L to l_e. We give this new Biot number the subscript e in reference to transport to the lower epidermis. The Biot number for the steady state 3D problem is then given by $\mathcal{B}_e^{3D} = h_v l_e / k_\ell^{3D}$, and the relationship between the 3D steady state Biot number and that of the related transient solution, from which k_ℓ^{3D} is determined, is just,

$$\mathcal{B}_e^{3D} = \mathcal{B}^{3D} \cdot \frac{l_e}{L}. \tag{37}$$

2.9. Analytic solution to the 1D steady state problem

For the 1D problem, as there is no flux to the upper epidermis, and the vascular conductance supplying the flux to the lower epidermis is then $2h = h_A$ (Figure 4) . We solve,

$$\frac{\partial^2\Psi}{\partial X^2} = 0, \tag{38}$$

$$\text{with BCs} : \frac{\partial\Psi}{\partial X}\Big|_{X=0} + \frac{h_A l_e}{k_\ell^{1D}}(1 - \Psi_{X=0}) = 0, \tag{39}$$

$$\Psi_{X=1} = 0. \tag{40}$$

The solution follows easily from two integrations and application of the boundary conditions,

$$\Psi = \frac{\mathcal{B}_e^{1D}}{1+\mathcal{B}_e^{1D}}(1-X), \qquad \mathcal{B}_e^{1D} = \frac{h_A l_e}{k_\ell^{1D}}. \tag{41}$$

For the steady-state numerical solution with any given $\mathcal{B}_e^{3D}$, its 1D approximation is given by the above according to,

$$\mathcal{B}_e^{1D} = \frac{h_A}{h_v}\mathcal{B}_e^{3D}. \tag{42}$$

2.10. Basis for steady-state model comparisons

We compare the two solutions by evaluating the magnitude of the total flux at the lower epidermal surface. Requiring that the numerical (3D) and analytic (1D) fluxes be equal leads to,

$$k_\ell^{3D}\frac{(\psi_r-\psi_e)}{l_e}\left\langle \frac{\partial\Psi}{\partial X}\Big|_{X=1}^{3D}\right\rangle = k_\ell^{1D}\frac{(\psi_r-\psi_e)}{l_e}\frac{\mathcal{B}_e^{1D}}{1+\mathcal{B}_e^{1D}}. \tag{43}$$

The angle brackets indicate an averaging operation, as introduced in (A.10), here applied to the gradient in Ψ at $X = 1$. From this we can construct two tests of how well the 1D steady-state solution concurs with the 3D steady-state solution. For the first case, we consider the true value of k_ℓ as well as $\psi_r - \psi_e$ to be known. The ratio of the 1D to 3D gradients is then equal to the ratio of the predicted fluxes, and the 1D model is well specified if that ratio is close to one, or

$$\frac{\mathcal{B}_e^{1D}}{1+\mathcal{B}_e^{1D}}\left\langle \frac{\partial\Psi}{\partial X}\Big|_{X=1}^{3D}\right\rangle^{-1} = \frac{J^{1D}}{J^{3D}} \approx 1. \tag{44}$$

For the second test, we take k_ℓ^{1D} to be defined by the 1D analysis of a transient experiment. We can then ask what the total error arising from reduction to 1D would be in estimating the driving force, the potential difference $\Delta\psi = \psi_r - \psi_e$, for an observed flux. For that case, the test is

$$\frac{k_\ell^{3D}}{k_\ell^{1D}}\frac{1+\mathcal{B}_e^{1D}}{\mathcal{B}_e^{1D}}\left\langle \frac{\partial\Psi}{\partial X}\Big|_{X=1}^{3D}\right\rangle = \frac{\Delta\psi^{1D}}{\Delta\psi^{3D}} \approx 1. \tag{45}$$

This second test incorporates both transient and steady-state sources of error arising from the assumption of a continuous vascular plane.

2.11. Test of an 'effective' tissue length in conjunction with a continuous vascular plane

To improve the continuous vascular plane assumption, one could consider an effective length through the tissue to attempt to slow down the 1D model to account for the true multidimensional nature of the flow. The specific hypothesis that has been suggested, and that we want to test, is that, for steady flow from the veins to the stomatal bearing surface the effective distance through the mesophyll is given by $D_{m,e} = \sqrt{l_e^2 + w^2}$, or the hypotenuse of a right triangle formed by the half thickness and half inter vein distance (Brodribb et al., 2007, 2010).

For the transient problem, where flow occurs both to the upper and lower surfaces, the average relevant length is $D_m = \sqrt{L^2 + w^2}$. Again, the vascular conductance to half the leaf thickness is just half the leaf area normalized vascular conductance, $h_A/2$. The Biot number for the 1D hypotenuse transient model, $\mathcal{B}_\triangle$, is then related to the Biot number of the numerical transient model by,

$$\mathcal{B}^\triangle = \mathcal{B}^{3D}\frac{h_A}{2h_V}\frac{D_m}{L}, \qquad \frac{h_A}{2h_V} = 4\frac{a}{w} - 3\frac{a^2}{w^2}. \tag{46}$$

As hydraulic capacity is normalized to the leaf volume $A\cdot 2L$, the introduction of a nominal length through the tissue requires a re-normalization of the hydraulic capacity if we are to conserve the number of water molecules ΔN absorbed during the transient, where $\Delta N = \Delta\psi(A2L)c_\ell$. Given a new nominal volume of $A\cdot 2D_m$, the rescaled capacity that conserves ΔN is then $c_\ell L/D_m$. The characteristic time for the 1D hypotenuse model becomes $\tau^\triangle = c_\ell L D_m/k_\ell$, and the test of the model is,

$$\frac{k_\ell^\triangle}{k_\ell^{3D}} = \frac{T_{1/2}^\triangle}{T_{1/2}^{3D}}\gamma\frac{D_m}{L}, \tag{47}$$

which says that the k_ℓ fitted by the 1D hypotenuse model will conform to that of the 3D numerical solution if the RHS equals one. The solution to the 1D model used to calculate $T_{1/2}^\triangle$ is as before, with $T^\triangle = t/\tau^\triangle$ and $\mathcal{B}^\triangle$ replacing T^{1D} and $\mathcal{B}^{1D}$ in (A.17).

For the 1D steady state problem in an hypostomatous leaf, the solution is as in (41), with $X = x/D_{m,e}$, and $\mathcal{B}_e^{1D}$ replaced by,

$$\mathcal{B}_e^\triangle = \frac{h_A D_{m,e}}{k_\ell}, \quad \text{or} \quad \mathcal{B}_e^\triangle = \frac{h_A}{h_V}\mathcal{B}_e^{3D}\frac{D_{m,e}}{l_e} \tag{48}$$

With k_ℓ considered perfectly known, the test of how well the 1D effective length model describes the gradient at the epidermis relative to the 3D solution becomes,

$$\frac{\mathcal{B}_e^\triangle}{1+\mathcal{B}_e^\triangle}\frac{l_e}{D_{m,e}}\left\langle \frac{\partial\Psi}{\partial X}\Big|_{X=1}^{3D}\right\rangle^{-1} \approx 1. \tag{49}$$

The test for how well the potential drop to the epidermis would be captured by this effective length idea, again combining errors arising from both 1D transient and 1D steady state analyses, becomes,

$$\frac{k_\ell^{3D}}{k_\ell^\triangle}\frac{1+\mathcal{B}_e^\triangle}{\mathcal{B}_e^\triangle}\frac{D_{m,e}}{l_e}\left\langle \frac{\partial\Psi}{\partial X}\Big|_{X=1}^{3D}\right\rangle = \frac{\Delta\psi^\triangle}{\Delta\psi^{3D}} \approx 1. \tag{50}$$

3. Results

3.1. Utility of the continuous vascular plane (CVP) 1D model

As w/L decreases across the four species modeled (*Acer*, *Tilia*, *Quercus rubra*, *Ailanthus*), the gradients in the 3D transient simulations become more one-dimensional, as can be seen qualitatively in a plot of the isopotential surfaces at the hydration halftimes (Figure 5). A similar effect of w/L can be seen in the isopotential surfaces of the steady state numeric solution

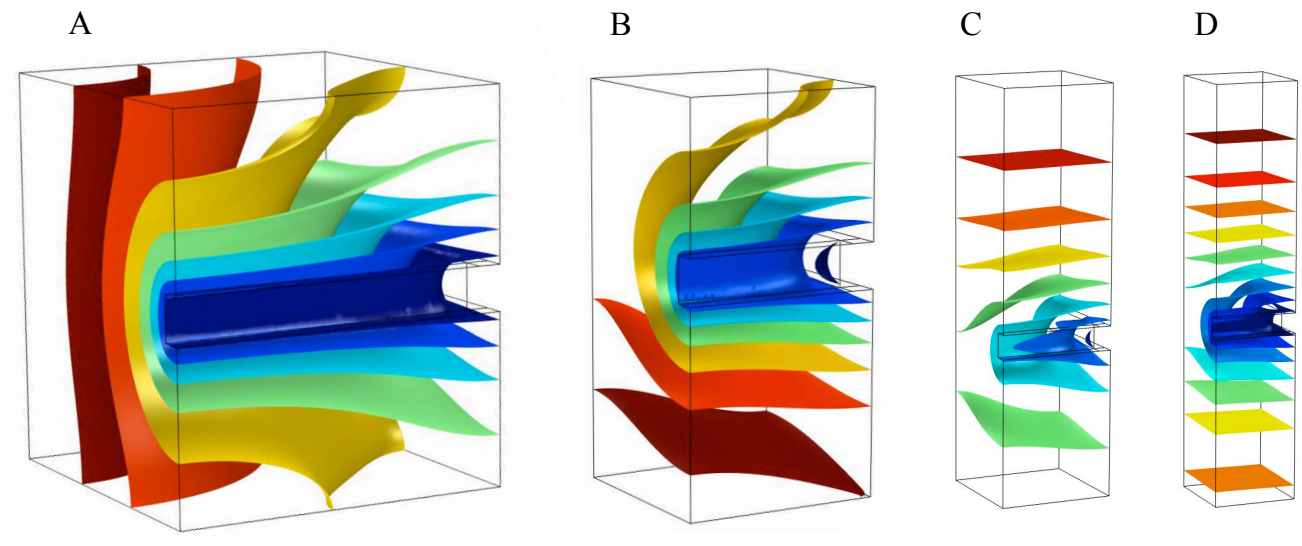

Figure 5: Numerical simulations of the isosurfaces of the potential field Ψ at the halftime of hydration in a quarter areole for four leaf geometries (Figure 2 B, Table 3), showing the increasingly 1D nature of the solution away from the veins with decreasing w/L. The color range shows the wettest (blue) to driest (maroon) potentials at the halftime: the shapes of the isosurfaces in each geometry are conserved for all Biot numbers, while the numeric scale associated with the color map varies across Biot numbers, as well as between geometries. However, by definition the average Ψ in every case is one half. **A**: *Acer saccharinum*; **B**: *Tilia americana*; **C**: *Quercus rubra*; **D**: *Ailanthus glandulosa*.

(Figure 6). As a result of this sensitivity to w/L, the test of the 1D transient model (eqn. 17) performs well for *Ailanthus glandulosa* over a larger range of $\mathcal{B}^{3D}$ values, falling within a $\pm 10\%$ tolerance over $\mathcal{B}^{3D} < 6$ (Figures 7 D, 5 D). Conversely, as w/L approaches two, as in *Acer saccharinum* (Figures 7 A, 5 A), the range over which the CVP assumption works well falls to $\mathcal{B}^{3D} < 0.5$. That is, the larger the gradients in Y, Z in the 3D solution, the less well the 1D CVP model predicts k_ℓ. Similarly, in the steady state model comparisons (eqn's 44, 45, Figure 7), the CVP 1D model does better the faster the isosurfaces in potential flatten in the Y, Z plane as one moves from the vein toward the lower surface (Figure 6). That in all cases the CVP 1D model converges with the 3D simulation at the lowest values of $\mathcal{B}^{3D}$ (Figure 7), arises simply from the fact that at those Biot numbers the solutions depend almost entirely on h_A, as the vasculature is the limiting resistance for the hydration of the tissue. The agreement in this limit, itself trivial, decays rapidly for the mid-range of Biot numbers as the halftimes become very sensitive to the exact value of the Biot number, and then asymptote to a near constant value as $\mathcal{B}^{3D}$ goes to infinity. This behavior also characterizes the 1D solution, as shown in Table A.1, where as $\mathcal{B}$ goes to infinity the solution approaches the limiting case of a fixed potential ψ_r at the vascular-tissue boundary.

That the ratio of 1D conductivity to 3D falls below one indicates that simply 'spreading' the vascular conductance over the vascular plane to reduce the dimensions of the flow to 1D, as in the CVP model, leads to a solution with too short a halftime (eqn. 17). The CVP model therefore tends to overestimate the total effective conductance of the vascular system, leading to an underestimate of k_ℓ. The CVP model similarly overestimates the steady state gradient at the epidermis, and so the flux (eqn. 44). As these two errors are in different directions, they partially offset each other in estimating the source to epidermis potential difference, though when the underestimate in the conductivity is large it forces large overestimates in the potential difference as well (eqn. 45).

3.2. Utility of the CVP plus effective tissue length 1D model

The results of transient, steady, and combined test are in Figure 8. For all geometries, the addition of an effective length improved the 1D CVP model with respect to the ratio of the conductivities and steady non-dimensional gradients. The improvement in the conductivity estimate came about not by increased congruence of the halftimes, but by the scaling of those times by the ratio of the length scales (eqn. 47). The same was also true for the ratio of the gradients (eqn. 49). However, as the net effect was for the gradients to be under-predicted, rather than over-predicted as by the CVP alone, the resulting errors were compounded in the estimate of the total potential drop (eqn. 50). As with the CVP alone, the CVP plus effective length strategy also improved with decreasing w/L. However, as $w/L < 1$, D_m approaches L, and the improvement with respect to the CVP alone model diminishes, as can be seen by comparing the results for *Ailanthus* (Figures 7 D, 8 D). Thus the adoption of the hypotenuse formed by L and w as an effective length to account for the discrete placement of veins, while resulting in some improvement, is still far from satisfactory in providing a consistent and accurate reduction of the 3D problem across a range of Biot numbers and leaf geometries.

3.3. Scaling factors for the transient models

Motivated by the 1D result of a simple linear relationship between $\mathcal{B}^{1D}$ and the quantity $\mathcal{B}^{1D} \cdot T_{1/2}^{1D}$ in (A.20), and the resulting approximate form (30), we sought similar relationships in the solutions to the 3D problem for $\mathcal{B}^{3D} = 0.1 \rightarrow 40$, for each

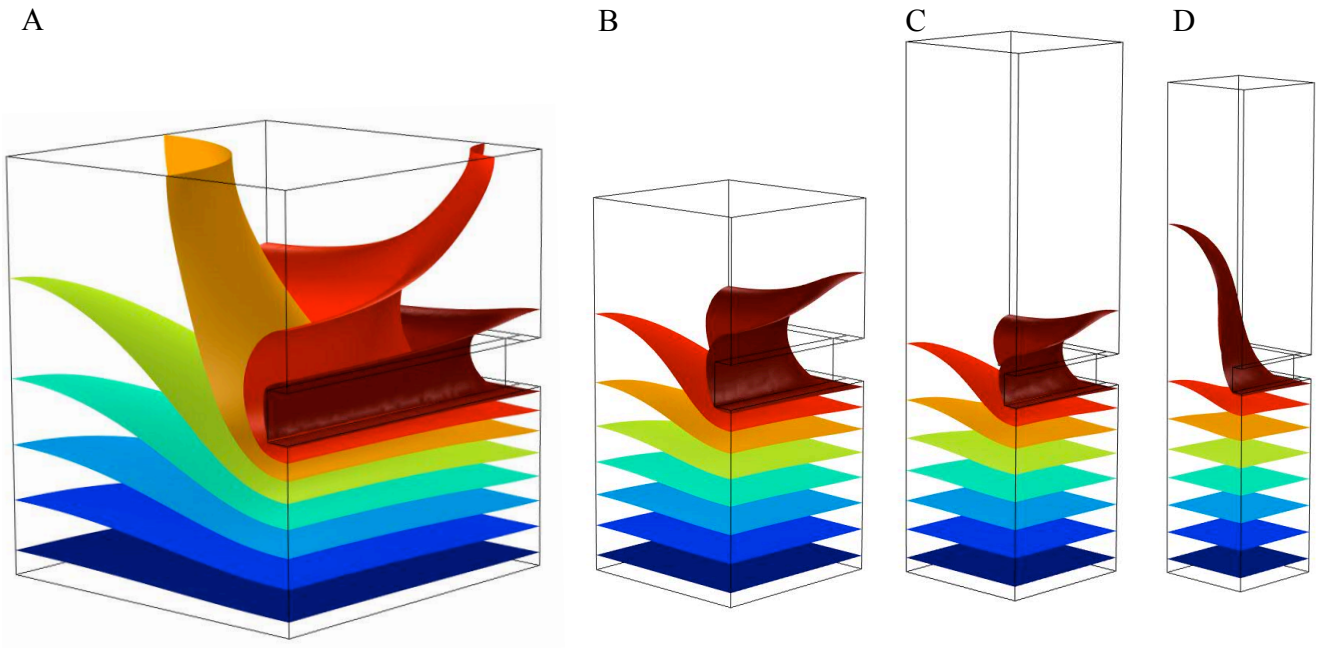

Figure 6: Numerical simulations of the isosurfaces of the steady potential field Ψ for four leaf geometries (Figure 2 B, Table 3), showing the increasingly 1D nature of the gradients as w/l_e decreases from left to right. The specific numeric values associated with the color map (blue = wet, maroon = dry) vary between geometries and with the Biot number, but the shapes of the isosurfaces are conserved across the range of Biot numbers for any particular leaf. Isosurfaces are evenly spaced, such that the absence of surfaces from the upper portion of some domains indicates a region of high homogeneity in potential. **A**: *Acer saccharinum*; **B**: *Tilia americana*; **C**: *Quercus rubra*; **D**: *Ailanthus glandulosa*.

of the 19 leaf geometries in Table 3. We found that a model of the form,

$$\mathcal{B}^{3D} T_{1/2}^{3D} = \alpha \mathcal{B}^{3D} + \beta \tag{51}$$

could be fit for each individual leaf geometry (i.e., α and β varied between species) with an $r^2 > 0.999$ (data not shown). As before, equation (51) re-arranges to

$$t_{1/2} = \alpha \tau^{3D} + \beta \frac{\tau^{3D}}{\mathcal{B}^{3D}}. \tag{52}$$

As $t_{1/2}$ is an experimental result, we can posit the existence of scaling factors ξ and η, such that the approximate analytic solution (31) set equal to the observed halftime correctly yields an estimate of k_ℓ equivalent to that fit by the 3D model. Setting these two expressions for $t_{1/2}$ equal yields,

$$\alpha \tau^{3D} + \beta \frac{\tau^{3D}}{\mathcal{B}^{3D}} = 0.197 \xi \tau^{1D} + 0.693 \eta \frac{\tau^{1D}}{\mathcal{B}^{1D}}. \tag{53}$$

Setting like terms equal yields two equations that define ξ and η as,

$$\xi = \frac{\alpha}{0.197} \frac{\tau^{3D}}{\tau^{1D}}, \qquad \eta = \frac{\beta}{0.693} \frac{\tau^{3D}}{\tau^{1D}} \frac{\mathcal{B}^{3D}}{\mathcal{B}^{1D}}. \tag{54}$$

The ratios of 3D to 1D τ and $\mathcal{B}$ have been previously identified. The scaling factors relating 3D to 1D halftimes, particular to a specific leaf geometry but independent of Biot number, are then

$$\xi = \frac{\alpha}{0.197} \frac{1}{\gamma}, \qquad \eta = \frac{\beta}{0.693} \frac{1}{\gamma} \frac{h_A}{2h_V}. \tag{55}$$

ξ and η for each leaf geometry are given in Table 3. Notably, η in all cases was very close to one, and may indeed be estimated as one, or the mean value of 1.033.

While we were then able to find a scaling for each leaf geometry that related the 3D simulation to a 1D solution, this is only really useful if one can avoid the necessity of running the numerical simulations and predict ξ for any leaf based on its geometry. To explore this possibility, we employed regression analysis, finding a strong linear dependence of ξ on both $D_m/L = \sqrt{1 + w^2/L^2}$ and w/L, with a slight advantage to the former. Knowledge of L and w therefore appears sufficient to find a good estimate of the 3D halftime with the re-scaled CVP 1D model for any Biot number (Figure 9 A, Table 4).

That a measure of the ratio of inter-vein distance to thickness does so well on its own may be due to a relative lack of variation in a in our data, the vein xylem half-width. Including a sensitivity to a into the model does however further improve the fit for leaves with relatively large or small vascular surface areas (Figure 9 B, Table 4). With regard to location of the veins in the thickness, values of vp larger or smaller than one half make hydration less efficient and slow down the halftime, including a term based on the absolute deviation of vp from one half did not result in any further improvement.

While ξ is fit to only one point on the time and potential curve, the scaling may be applied to the whole relaxation curve described by inverting the approximate solution (27). Replacing the time dimension into the equation then yields hydration time as a function of Ψ,

$$t = \xi \frac{4}{\pi^2} \ln\left(\frac{8}{\Psi \pi^2}\right) \frac{c_\ell^{1D} L^2}{k_\ell^{1D}} - \eta \ln(\Psi) \frac{2 c_\ell^{1D} L}{h_A}. \tag{56}$$

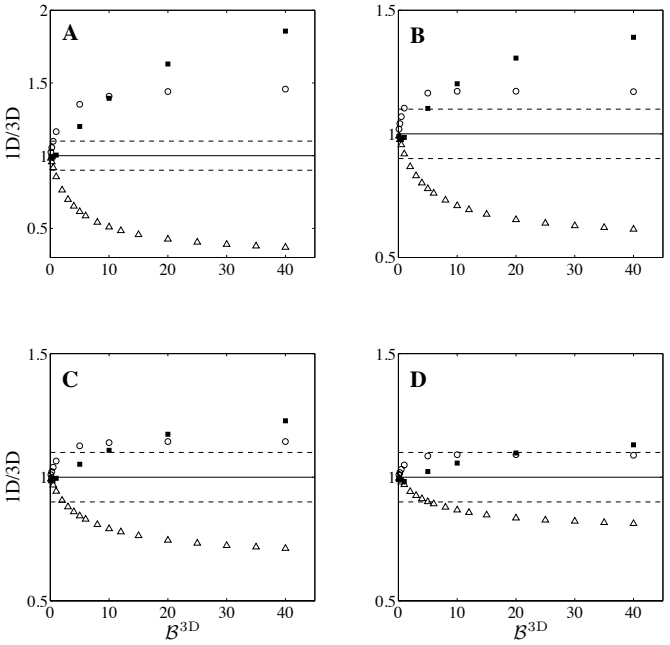

Figure 7: Comparison of the 3D and 1D solutions, using an effective vascular conductance h, as a function of the Biot number $\mathcal{B}^{3D}$ for four leaf geometries in order of decreasing w/L. Triangles are the ratio k_ℓ^{1D}/k_ℓ^{3D} from the transient solutions (eqn. 17). From the steady state solutions, circles are the ratio of the predicted fluxes (eqn 44), filled squares the ratio of the predicted potential drops to the lower epidermis (eqn. 45). Dashed lines are drawn at 0.9 and 1.1, bounding the region in which errors are less than 10%. **A**: *Acer saccharinum*; **B**: *Tilia americana*; **C**: *Quercus rubra*; **D**: *Ailanthus glandulosa*.

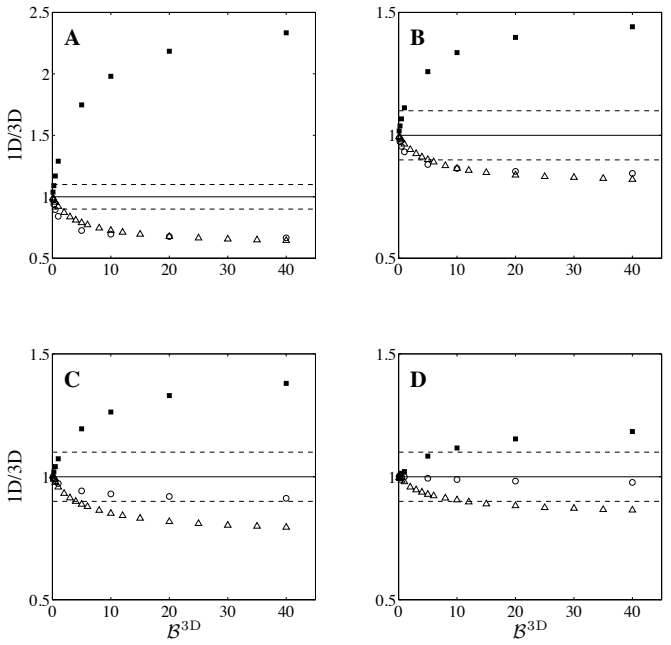

Figure 8: Comparison of the 3D and 1D solutions using the effective length idea of Brodribb et al. (2007), as a function of the Biot number $\mathcal{B}^{3D}$ for four leaf geometries in order of decreasing w/L. Triangles are the ratio $k_\ell^{\triangle}/k_\ell^{3D}$ from the transient solutions (eqn. 47). From the steady-state solutions, circles are the ratio of the predicted fluxes (eqn. 49), filled squares the ratio of the predicted potential drops to the lower epidermis (eqn. 50). Dashed lines are drawn at 0.9 and 1.1, bounding the region in which errors are less than 10%. **A**: *Acer saccharinum*; **B**: *Tilia americana*; **C**: *Quercus rubra*; **D**: *Ailanthus glandulosa*.

Where k_ℓ is the parameter of interest, re-arrangement leads to

$$k_\ell^{1D} = \xi \frac{4}{\pi^2} \ln\left(\frac{8}{\Psi\pi^2}\right) \frac{c_\ell^{1D} L^2}{t + \eta \ln(\Psi) \frac{2c_\ell^{1D} L}{h_A}}. \tag{57}$$

To investigate how well the the scaled 1D model captures the full numeric relaxation curve, and therefore how well (57) will perform for values of $\Psi \neq 0.5$, we plotted the numeric equilibrium relaxation curve versus (56) scaled to the numeric time scale, or

$$T^{3D} = \gamma\xi \frac{4}{\pi^2} \ln\left(\frac{8}{\Psi\pi^2}\right) - \gamma\eta \frac{\ln(\Psi)}{\mathcal{B}^{1D}}, \tag{58}$$

with the values for ξ and η given in Table 3. We also plot the curve given by scaling T in (A.5) by $\gamma\xi$ and retaining the first five terms, and inverting the expression using the 'FindRoot' function in Mathematica 8 (Wolfram research Inc., Champaign, IL, USA) to find the tissue contribution to the total time as a function of Ψ. The resulting curves are in Figure 10. For the range of leaf geometries represented by *Acer*, *Tilia*, and *Ailanthus*, agreement between the scaled 1D and 3D curves in the region of experimental interest where the solution is not overly sensitive to either measurement errors in time or potential, from $\Psi = 0.7 \rightarrow 0.3$, was excellent over the range of $\mathcal{B}^{3D}$. For $\mathcal{B}^{3D} = 0.1$, both forms of the 1D model fully overlap as the vascular time dominates. At $\mathcal{B}^{3D} = 40$, the more one dimensional 3D solution of *Ailanthus*, due to its low w/L ratio, leads to near perfect agreement between the 1D and 3D curves even below $\Psi = 0.3$.

3.4. Empirical scaling factors for the steady state models

For the steady state potential gradients at the lower epidermis, we posit the existence of some scaling factor ς for the one dimensional Biot number such that,

$$\frac{\varsigma\mathcal{B}_e^{1D}}{1 + \varsigma\mathcal{B}_e^{1D}} = \left\langle \frac{\partial\Psi}{\partial X}\Big|_{X=1}^{3D} \right\rangle. \tag{59}$$

Regression of ς on $\mathcal{B}_e^{1D}$, based on data from the numeric solutions with $\mathcal{B}^{3D} = 0.1 \rightarrow 40$, provides a linear relation ($r^2 > 0.998$) for all leaf geometries of the form,

$$\varsigma^{-1} = \zeta\mathcal{B}_e^{1D} + \epsilon, \tag{60}$$

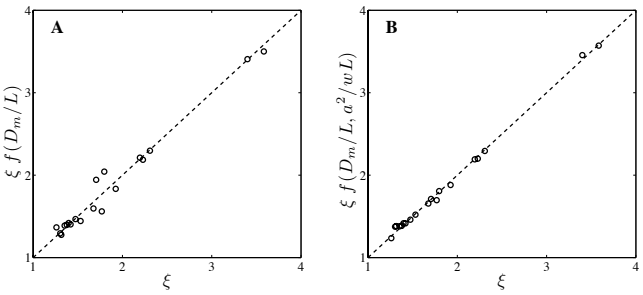

Figure 9: Predicting the scaling factor ξ that maps the 3D transient problem to a 1D solution using leaf geometry. **A**: ξ versus the value predicted by linear regression on D_m/L, ($r^2 = 0.974,\ n = 19$). **B**: ξ versus a model including both D_m/L and a^2/wL, ($r^2 = 0.997,\ n = 19$).

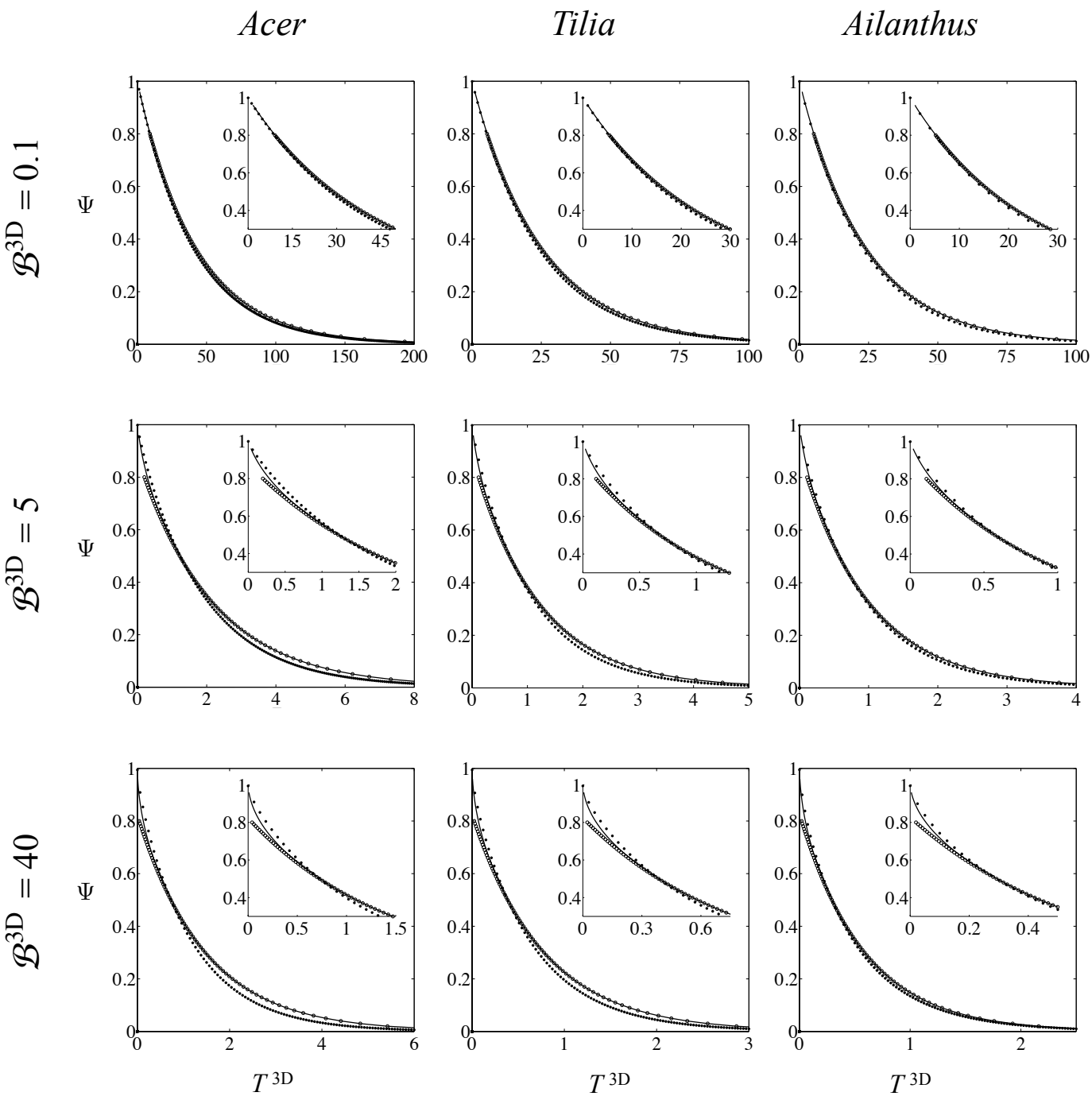

Figure 10: Potential relaxation curves showing equilibrium whole leaf potential Ψ as a function of hydration time T^{3D}, for three different leaf geometries and values of the Biot number. Closed circles represent the numeric simulations, open circles the scaled 1D approximate solution (eqn. 58), and solid line the 1D solution found by retaining 5 terms and inverting the series solution for $\Psi(T)$ (eqn. A.17) with the time variable re-scaled to $T\gamma\xi$. Insets highlight the fit in the region most useful for fitting k_ℓ, from about $\Psi = 0.7$, where all three curves converge, to about $\Psi = 0.2$, after which small errors in potential determination may begin to strongly influence parameter estimates. The largest errors are in the tail of the *Acer* $\mathcal{B}^{3D} = 40$ curve, below $\Psi = 0.3$, which reach as high as 17%.

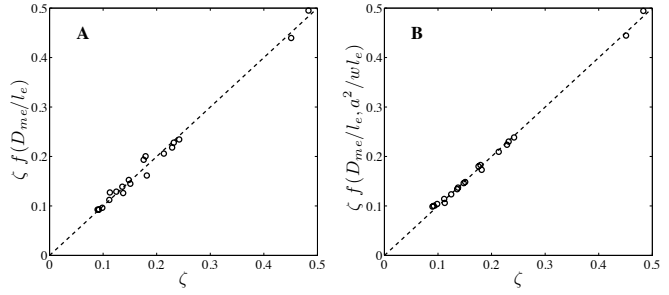

Figure 11: Predicting the scaling factor ζ that maps the 3D steady problem to a 1D solution using leaf geometry. **A**: ζ versus the value predicted by linear regression on $D_{m,e}/l_e$, ($r^2 = 0.99,\ n = 19$). **B**: ζ versus a model including both $D_{m,e}/l_e$ and a^2/wl_e, ($r^2 = 0.997,\ n = 19$).

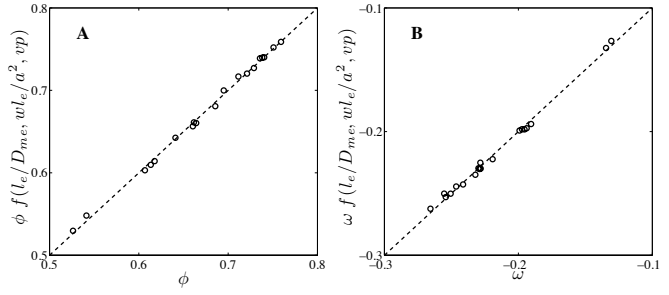

Figure 12: Modeling the parameters ϕ and ω that relate $\mathcal{B}_e^{1D}$ to $<\Psi>$, which sets the scaling between the average potential in the leaf and the total source to lower epidermis potential difference driving a steady flux. **A**: ϕ versus the value predicted by linear regression on $l_e/D_{m,e}$, wl_e/a^2, vp ($r^2 = 0.997,\ n = 19$). **B**: ω versus the value predicted by linear regression on $l_e/D_{m,e}$, wl_e/a^2, vp ($r^2 = 0.995,\ n = 19$).

which leads directly to a scaling between the 1d and 3D models for all values of the Biot number,

$$\frac{\mathcal{B}_e^{1D}}{\epsilon + (1+\zeta)\,\mathcal{B}_e^{1D}} = \left\langle \frac{\partial \Psi}{\partial X}\Big|_{X=1}^{3D} \right\rangle. \tag{61}$$

Fitted values of ζ and ϵ for each leaf geometry are given in Table 3. As with η, ϵ may be approximated as one, or taken as its average value of 1.037. Regression of ζ on the geometry of the steady state problem yielded a strong dependence on $D_{m,e}/l_e$ (Figure 11 A, Table 4 A), and as before adding a term sensitive to a further improved the fit (Figure 11 B, Table 4 B).

We can use the above result to estimate epidermal water potential when source potential for a leaf and the flux are both known. The relationship between an observed flux and the scaled 1D solution is given by,

$$\frac{Jl_e}{k_\ell^{1D}\,(\psi_r - \psi_e)} = \frac{\mathcal{B}_e^{1D}}{\epsilon + (1+\zeta)\,\mathcal{B}_e^{1D}}, \tag{62}$$

leading to an expression for epidermal water potential as,

$$\psi_e = \psi_r - \frac{Jl_e}{k_\ell^{1D}} \frac{\epsilon + (1+\zeta)\,\mathcal{B}_e^{1D}}{\mathcal{B}_e^{1D}}. \tag{63}$$

3.5. Parameters relating epidermal water potential to equilibrium whole leaf measurements

As current technology allows only equilibrium water potential measurements on whole leaves or tissues, a natural question is how such measurements relate to the total gradient in potential across the leaf, $\psi_r - \psi_e$. While ψ_r is known in the lab, or is available from potential measurements on bagged (non-transpiring) leaves that record stem potential, ψ_e is not generally directly obtainable. By definition, at steady state the average non-dimensional potential of the tissue domain in the 3D simulation, $<\Psi>$, is related to the average dimensional potential from an equilibrium measurement, $<\psi>$, by

$$<\Psi>\,(\psi_r - \psi_e) + \psi_e = <\psi>, \tag{64}$$

which leads directly to,

$$\psi_e = \frac{<\psi> - <\Psi>\,\psi_r}{1 - <\Psi>}. \tag{65}$$

Following our previous approach, to develop an equation to predict $<\Psi>$ we sought a linear relationship for each leaf geometry between $\mathcal{B}_e^{1D}$ and $\mathcal{B}_e^{1D}\ <\Psi>$. For numeric solutions over the given range of Biot numbers, the resulting fit for all leaf geometries had a minimum $r^2 = 0.998$ (Figure 12). With ϕ as the slope and ω the intercept of each regression, the average non-dimensional potential of the tissue in the steady state solution for any Biot number is given by

$$<\Psi> = \phi + \frac{\omega}{\mathcal{B}_e^{1D}}, \tag{66}$$

where the values of ϕ and ω for each geometry are reported in Table 3. We then regressed ϕ and ω versus leaf geometry, with the resulting models given in Table 4. As before, both a measure of the width to length ratio for the steady problem and relative vascular area contribute to the model, but unlike the previous two cases the location of the vascular plane vp needed to be included to fully explain the variation between leaves. This can be understood as arising from a need to account for the amount of tissue above the vascular plane that sits close to vascular potential, and which will therefore pull the average potential of the tissue closer to that of the vascular-tissue interface.

To estimate k_ℓ from steady state experiments, we can eliminate ψ_e by setting (63) and (65) equal to each other, such that with $<\psi>$ measured by the pressure chamber, k_ℓ remains the only unknown. However, as k_ℓ appears four times, the resulting equality cannot be reduced to a simple expression for k_ℓ, and therefore is best solved by computer (Matlab or Mathematica code is available from the corresponding author).

4. Discussion

Given the proliferation of terms, approximations, and idealizations in going from general conservation laws to the approximate 1D scaled solution (56), it may be useful to briefly summarize them here. The definition of k_ℓ rests on local equilibrium between cell symplast and apoplast, as well as with the adjacent intercellular airspace, as discussed previously (Rockwell

Table 4: Regression of 3D to 1D scaling factors on leaf geometry, (n = 19).

Factor	Model	F-stat	r^2
$\xi\ \left(\frac{D_m}{L}\right)$	$2.2286\left(1+\frac{w^2}{L^2}\right)^{1/2}-1.1093$	637.93	0.974
$\xi\ \left(\frac{D_m}{L},\frac{a^2}{wL}\right)$	$2.2832\left(1+\frac{w^2}{L^2}\right)^{1/2}-46.5422\frac{a^2}{wL}-0.8068$	2697.20	0.997
$\zeta\ \left(\frac{D_{m,e}}{l_e}\right)$	$0.3599\left(1+\frac{w^2}{l_e^2}\right)^{1/2}-0.3107$	1702.30	0.990
$\zeta\ \left(\frac{D_{m,e}}{l_e},\frac{a^2}{wl_e}\right)$	$0.3567\left(1+\frac{w^2}{l_e^2}\right)^{1/2}-3.7469\frac{a^2}{wl_e}-0.271$	3032.20	0.997
$\phi\ \left(\frac{l_e}{D_{m,e}},\frac{wl_e}{a^2},vp\right)$	$0.4086\left(1+\frac{w^2}{l_e^2}\right)^{-1/2}-0.0004\frac{wl_e}{a^2}+0.4201vp+0.1766$	1891.90	0.997
$\omega\ \left(\frac{l_e}{D_{m,e}},\frac{wl_e}{a^2},vp\right)$	$-0.3045\left(1+\frac{w^2}{l_e^2}\right)^{-1/2}+0.0004\frac{wl_e}{a^2}+0.0896vp-0.0895$	966.30	0.995

et al., 2014). The most important approximation introduced in this paper is the representation of the vascular network by a single average conductance to the vein-tissue interface, h_A. Relevant data are scarce, but for the leaves of *Tradescantia* Ye et al. (2008) found little variation in the half times of cells located at different vascular distances in response to a pressure pulse at the petiole. As long as leaf water potential measurements are made after the leaf has come to internal equilibrium, defining an average vascular conductance feeding the tissue is also consistent with the whole leaf averaging in experimental determinations of h_A from steady flow experiments, in which a whole leaf liquid flux is driven across the leaf vascular network immersed in a reservoir of water at atmospheric pressure. The greatest difficulty in decomposing leaf hydraulics into vascular and tissue components may be encountered in obtaining this estimate of h_A. In cutting veins, it can be difficult to ensure that only the intended order are severed (Sack et al., 2004), and a large number of cuts are necessary to saturate the response (Cochard et al., 2004). However, cutting of the tertiary vein order presents fewer difficulties, and may set a useful upper bound on h_A.

As the Biot number represents the ratio of vascular conductance to the conductance of a given length of tissue, it is natural to ask how this number relates to the question of whether vascular or tissue resistances dominate in leaves, the question motivating the vein cutting experiments discussed above. These studies idealized leaves as two discrete (i.e., Ohm's law) resistances in series, an average vascular resistance from the petiole to highest vein order followed by a tissue resistance; the latter is then bypassed by vein cutting, or removed by treatments to disrupt tissue membranes, and resulted in some controversy (Cochard et al., 2004; Sack et al., 2002; Salleo et al., 2003). Yet, this 1D conception allows no role for vein spacing, which has been recognized as an important correlate of high transpiration and rehydration rates (Boyce et al., 2009; Brodribb et al., 2010). Nor in our analysis does the Biot number itself, in either the 3D or 1D form, capture the effects of vein spacing: as we have shown the ratio of w to L has a strong effect on hydration times, independent of $\mathcal{B}$. The question then arises whether the 1D scaled models presented here might inform this debate.

That the important scaling factor for the transient problem in (56), ξ, acts on the tissue time suggests it is more natural to quantify the effect of vein spacing in terms of its impact on the time for flow within the tissue, rather than through the vasculature. Yet, the scaling factor introduced for the steady state problem ς, itself a function of the Biot number, can be interpreted as a rescaling of the vascular conductance h_A to account for the multidimensionality of the flow. Thus while the scaling factors identified here each have a specific utility, they are in no way guaranteed to be generalizable beyond the specific relations for which they are defined, and no completely general mapping of transport in a leaf to 1D appears to exist. The simple series conception of vascular and tissue resistances should perhaps therefore be retired in favor of analyzing leaf hydraulic architecture in terms of models that explicitly account for the topology of the vein-tissue interface. Some authors have already taken this approach.

Based on a 2D PDMS leaf analogue, Noblin et al. (2008) showed that increasing channel density increased the flux for a given driving force, as the gradients through the gel became more 1D. As the response saturates as channel density becomes high, this result leads to an optimal spacing argument that the inter-vein distance should be equal to the distance from the vascular plane to the lower epidermis ($d \approx \delta$, in their notation). For the survey data cited here, we estimate the mean for this ratio as 2.2, with a range of 1 to 4.7. Given that for leaves with net venation the minimum domain for analysis is 3D, the deviation from a 2D theory is perhaps unsurprising: when considering a quarter section of an areole, where flow occurs over two sides, the width at which diminishing returns to increasing vein density sets in will be higher than that suggested by a 2D view. We have not attempted an optimization analysis in this study, in part because we do not expect that leaf hydraulics are optimized for the isothermal rehydration problem principally considered here. Nevertheless, the approach to the 3D problem outlined here could be adapted to address questions of optimality in future.

What we have done in this study is to develop three 1D equations that, as they can be scaled to the 3D solution with knowledge of the geometry, can be used to characterize leaf hydraulic function in terms of continuum properties. Equation (57) defines a tissue hydraulic conductivity from transient experiments, which avoids the current practice of assuming lumped capacity approximation, the conditions for which are unlikely to be met

by leaves operating in their normal physiological range of water contents. Equation (63) relates this same parameter to steady state experiments, providing a common basis for comparing the results of steady and transient experiments that plant physiologists currently lack. Equation (65) then extends these results by relating them to $<\psi>$, the average potential of the leaf removed from steady state, as measured in the pressure chamber. As all the parameters are related clearly to material properties, this presents a considerable advance over the current practice of defining a nominal leaf conductance based on the relation $K_{leaf} = J/(\psi_r - <\psi>)$. However it must be emphasized that these results only apply to peristomatal evaporation (Meidner, 1975; Maier-Maercker, 1983), or where thermal gradients are not important in driving an internal vapor phase flux. While peristomatal evaporation is a common assumption (Brodribb et al., 2010), others see a dominant role for vapor transport (Mott and Peak, 2011), and gradients in saturated vapor pressure may lead to significant fluxes in the intercellular air spaces (Pieruschka et al., 2010). The hydraulic conductivity of the tissue in this analysis, k_ℓ, accounts for vapor transport due to gradients in saturated vapor pressure in the intercellular air spaces resulting from water potential gradients in the adjacent cells (**?**), and so iso-thermal vapor transport, but not thermal effects. The non-isothermal problem will be taken up in a subsequent analysis.

With respect to the relations between the 1D and 3D scaling factors and leaf geometry, quite reasonable estimates for ξ and ζ can be made based on L and w alone, neglecting vp and a.This may be because of relatively low variation in bundle sheath cell radius, from which we estimated a, in the leaf geometries considered. While we expect the geometry of most woody angiosperms to fall within the geometrical parameter space considered, extrapolation of these relationships to geometries outside the range, particularly for gymnosperms with very large vascular bundles and for which the requisite domain may be 2D by symmetry, is not recommended. In addition, at long hydration times, as Ψ falls below about 0.3, the kinetics of hydration toward equilibrium with pure water at atmospheric pressure slow dramatically (Boyer, 1968; Zwieniecki et al., 2007). Processes implicated in such bi-phasic phenomena include growth (Boyer, 1968), flooding of intercellular air spaces (Rockwell, 2010), hydraulic compartmentation (Zwieniecki et al., 2007), and the accumulation of solutes at the xylem-tissue interface (Knipfer et al., 2007). The models discussed here do not account for such effects. Rather, they provide the simplest possible descriptions of leaf hydration that capture the effect of vein spacing, and do so in terms of parameters that may then be directly related to the average hydraulic properties of a leaf's cells (**?**).

Appendix A. Solutions to the unsteady 1D problem as a function of the Biot number

Appendix A.1. $\mathcal{B}^{1D} \gg 1$

In the limit that conductance through the vasculature is much greater than through the tissue we have

$$\mathcal{B}^{1D} = \frac{hL}{k_\ell^{1D}} \gg 1, \qquad \Psi\left(X = 0, T^{1D} > 0\right) \to 0. \tag{A.1}$$

Since the non-dimensionalized flux, the first term in (26), is at most order one, then to satisfy the full expression in (26), the term $\mathcal{B}^{1D}\Psi(X = 0)$ can be at most order one; thus, if $\mathcal{B}^{1D} \gg 1$, $\Psi(X = 0)$ must become much less than one. In this limit, we can approximate (26) with the more tractable boundary condition

$$\Psi\left(X = 0, T^{1D} > 0\right) \approx 0. \tag{A.2}$$

This is the form assumed by (Boyer, 1968), where the vascular plane is treated as a homogeneously wet layer held at a potential fixed for all time by an external reservoir. Solutions to this class of problem are given by Crank (1957), and the representation of the potential field through the half thickness of the leaf is then given by

$$\Psi(X, T^{1D}) = \sum_{n=0}^{\infty} \frac{4}{(2n+1)\,\pi} \sin\left(\lambda_n X\right) \exp\left(-\lambda_n^2 T^{1D}\right), \tag{A.3}$$

where the λ_n's are given by,

$$\lambda_n = \left(\frac{2n+1}{2}\right)\pi. \tag{A.4}$$

When the leaf has hydrated for t seconds and then is allowed to come to internal equilibrium, the potential of the leaf is given by

$$\Psi(T^{1D}) = \frac{8}{\pi^2} \sum_{n=0}^{\infty} \frac{\exp\left(-\lambda_n^2 T^{1D}\right)}{(2n+1)^2}. \tag{A.5}$$

The cumulative uptake Q, in moles of water molecules over the entire leaf (upper and lower halves), can be found by evaluating two times the flux from the vasculature to the tissue (at $x = 0$), times the area of the leaf, and integrating up to time t.

$$Q(T^{1D}) = 2A_\ell \int_0^t J\Big|_{X=0}\, dt = \\ - 2A_\ell k_\ell \frac{(\psi_o - \psi_r)}{L} \tau \int_0^{T^{1D}} \frac{\partial \Psi}{\partial X}\Big|_{X=0} dT^{1D}. \tag{A.6}$$

The non-dimemsionalized uptake is then,

$$\Phi(T^{1D}) = \frac{Q(T^{1D})}{(\psi_r - \psi_o)\, V_\ell c_\ell} = \frac{8}{\pi^2} \sum_{n=0}^{\infty} \frac{1 - \exp\left(-\lambda_n^2 T^{1D}\right)}{(2n+1)^2}, \tag{A.7}$$

where the first equality defines Φ as the non-dimensionalized uptake, normalized by the expected uptake given by the water potential difference between two equilibrium states, the leaf volume and hydraulic capacity.

The series solutions for diffusion type equations given by (A.5) or (A.7) result in sums of individual exponential terms that decay fairly rapidly with n, such that as few as 10 terms need actually be evaluated (Crank, 1957). We can then find the halftime for relaxation (or uptake) by setting the left hand side of (A.5) or (A.7) to 0.5 and solving for T^{1D}, with the result that $T^{1D}_{1/2} = 0.197$.

In addition, individual terms of the series also decrease as times goes on (Crank, 1957), such that after about $0.14\,\tau^{1D}$ the potential is well approximated by the $n = 0$ term alone,

$$\frac{\psi(t) - \psi_r}{\psi_o - \psi_r} \approx \frac{8}{\pi^2} \exp\left(-\frac{\pi^2}{4}\frac{k_\ell}{c_\ell L^2} t\right). \tag{A.8}$$

Since τ^{1D}, and therefore $0.14\,\tau^{1D}$, will in general be unknown prior to experiment, the latter may not provide a useful guide as to when (27) may be used. However, recalling the definition of the halftime, $t_{1/2} = 0.197\,\tau^{1D}$, as $0.197\,\tau^{1D} > 0.14\,\tau^{1D}$ we expect that (27) provides a reasonable approximation to the full solution when the potential change in an experiment approaches half the initial value.

Appendix A.2. $\mathcal{B}^{1D} \ll 1$

In the limit $\mathcal{B}^{1D} \ll 1$, since the magnitude of Ψ can be at most 1, the term $\mathcal{B}^{1D}\Psi$ tends towards zero. In order to satisfy (26) this requires that the gradient of Ψ in X must also vanish. Physically, this means that when transport through the tissue becomes very fast relative to through the vasculature, the gradient through the tissue becomes vanishingly small. In this limit the potential anywhere in the tissue approaches the average potential in the tissue, $<\Psi>$, defined by

$$<\Psi> = \int_0^1 \Psi \mathrm{d}X. \tag{A.9}$$

We next write equation 23 in terms of the average potential:

$$\frac{\partial <\Psi>}{\partial T^{1D}} = \int_0^1 \frac{\partial^2 \Psi}{\partial X^2}\mathrm{d}X = -\mathcal{B}\Psi\left(X = 0, T^{1D} > 0\right). \tag{A.10}$$

The last equality follows from application of the boundary conditions, (25) and (26).

If we now assert that $<\Psi> \approx \Psi\left(X = 0, T^{1D} > 0\right)$, we arrive at

$$\frac{\partial \Psi}{\partial T^{1D}} = -\mathcal{B}^{1D}\Psi, \qquad \text{with I.C.} \quad \Psi(t \le 0) = 1. \tag{A.11}$$

Consequently, the tissue of the leaf can be represented by a single potential following first order kinetics. The lumped capacity solution for the leaf water potential is then just,

$$\Psi(T^{1D}) = \exp\left(-\mathcal{B}^{1D}T^{1D}\right), \quad \mathcal{B}^{1D}T^{1D} = \frac{\mathcal{B}^{1D}}{\tau^{1D}}t = \frac{h}{c_\ell^{1D} L}t. \tag{A.12}$$

Note that the time scale of the solution in this limit is $\tau/\mathcal{B}^{1D}$. The solution for uptake follows as,

$$\Phi(T^{1D}) = \frac{Q(T^{1D})}{(\psi_r - \psi_o)\, V_\ell c_\ell} = 1 - \exp\left(-\mathcal{B}^{1D}T^{1D}\right). \tag{A.13}$$

With $c_A = 2L \cdot c_\ell$ as the capacitance of the leaf per unit leaf area, and $2h = K_\ell$, (28) is the form adopted by (Brodribb and Holbrook, 2004) for quantifying the susceptibility of leaf xylem to cavitation, a limit in which we can indeed expect vascular resistance to dominate that of the tissue. As vascular resistance increases due to embolism, a leaf may indeed approach an ohmic RC circuit. Specifically, if the declines in h arise due to cavitation in the petiole, or homogeneously in the finest veins, then (A.11) represents the 'lumped capacity' solution in which all the cells hydrate with a single time scale, given by c_A/K_ℓ.

Even in the case of heterogeneous cavitation within the vasculature of the blade, (A.11) provides a useful index of hydraulic impairment, as long as all potential measurements are made at equilibrium. That is, for (A.11) to be consistently applied we required $<\Psi> \approx \Psi(X = 0)$, which tells us we need to wait to make post-rehydration water potential measurements until redistribution from hydraulically well-connected areas of the leaf to those isolated by embolism has occurred, and the leaf is again described by a single equilibrium potential, as in the pre-hydration state. In this limit, setting (28) or (A.13) equal to 0.5 yields the halftime,

$$t_{1/2} = 0.693\frac{\tau^{1D}}{\mathcal{B}^{1D}}. \tag{A.14}$$

Appendix A.3. $\mathcal{B}^{1D} \sim 1$

When conductance through the vasculature neither dominates nor is negligible compared to the conductance through a half thickness of the tissue, we must solve (23) subject to the un-reduced boundary condition (26); a general approach is described by Carslaw and Jaeger (1959). Solving (23) subject to (24, 25, 26), the potential field is given by,

$$\Psi(X, T^{1D}) = \sum_{n=1}^{\infty} \frac{2(\mathcal{B}^{1D} - \mathcal{B}^{1D}\cos\lambda_n + \lambda_n \sin\lambda_n)}{\mathcal{B}^{1D} + (\mathcal{B}^{1D})^2 + \lambda_n^2} \left[\cos\lambda_n X + \frac{\mathcal{B}^{1D}}{\lambda_n}\sin\lambda_n X\right] \exp\left(-\lambda_n^2 T^{1D}\right). \tag{A.15}$$

The λ_n's are given by the positive real roots of

$$\lambda - \mathcal{B}^{1D}\cot\lambda = 0, \tag{A.16}$$

which may be numerically calculated. The equilibrium potential of the leaf after t seconds of hydration is given by,

$$\Psi(T^{1D}) = \sum_{n=1}^{\infty} \frac{2(\mathcal{B}^{1D} - \mathcal{B}^{1D}\cos\lambda_n + \lambda_n \sin\lambda_n)^2}{(\mathcal{B}^{1D} + (\mathcal{B}^{1D})^2 + \lambda_n^2)\,\lambda_n^2} \exp\left(-\lambda_n^2 T^{1D}\right). \tag{A.17}$$

The cumulative uptake of water, found by evaluating the flux into the tissue in the same manner as for (A.6), is then,

$$\Phi(T^{1D}) = \frac{Q(T^{1D})}{(\psi_r - \psi_o)\, V_\ell c_\ell} = \sum_{n=1}^{\infty} \frac{2\mathcal{B}^{1D}(\mathcal{B}^{1D} - \mathcal{B}^{1D}\cos\lambda_n + \lambda_n \sin\lambda_n)}{(\mathcal{B}^{1D} + (\mathcal{B}^{1D})^2 + \lambda_n^2)\,\lambda_n^2} \left(1 - \exp\left(-\lambda_n^2 T^{1D}\right)\right). \quad \text{(A.18)}$$

As in the previous case, the contributions from each λ_n die off both with increasing n and t. Table A.1 shows the dominant surviving term after about $0.14\,\tau^{1D}$, as well as the halftimes for a range values of $\mathcal{B}^{1D}$. Halftimes for uptake and relaxation for a particular value of $\mathcal{B}^{1D}$ were found as before, by setting (A.17) or (A.18) equal to 0.5, retaining the first ten terms of the series, and then solving for $T^{1D}_{1/2}$, the value of T^{1D} when $\Psi = 0.5$.

Table A.1: Solutions for long times as a function of $\mathcal{B}^{1D}$

$\mathcal{B}^{1D}$	Dominant Term	Halftime
0.1	$0.999\exp(-0.097\,T^{1D})$	$7.162\,\tau^{1D}$
0.5	$0.996\exp(-0.427\,T^{1D})$	$1.614\,\tau^{1D}$
0.75	$0.991\exp(-0.595\,T^{1D})$	$1.150\,\tau^{1D}$
1	$0.986\exp(-0.740\,T^{1D})$	$0.918\,\tau^{1D}$
1.25	$0.981\exp(-0.866\,T^{1D})$	$0.777\,\tau^{1D}$
1.5	$0.975\exp(-0.977\,T^{1D})$	$0.684\,\tau^{1D}$
1.75	$0.969\exp(-1.074\,T^{1D})$	$0.616\,\tau^{1D}$
2	$0.964\exp(-1.160\,T^{1D})$	$0.566\,\tau^{1D}$
2.5	$0.953\exp(-1.305\,T^{1D})$	$0.494\,\tau^{1D}$
3	$0.943\exp(-1.422\,T^{1D})$	$0.446\,\tau^{1D}$
3.5	$0.934\exp(-1.518\,T^{1D})$	$0.412\,\tau^{1D}$
4	$0.926\exp(-1.599\,T^{1D})$	$0.386\,\tau^{1D}$
4.5	$0.919\exp(-1.668\,T^{1D})$	$0.365\,\tau^{1D}$
5	$0.913\exp(-1.726\,T^{1D})$	$0.349\,\tau^{1D}$
6	$0.902\exp(-1.821\,T^{1D})$	$0.324\,\tau^{1D}$
7	$0.893\exp(-1.895\,T^{1D})$	$0.307\,\tau^{1D}$
8	$0.886\exp(-1.954\,T^{1D})$	$0.293\,\tau^{1D}$
9	$0.880\exp(-2.002\,T^{1D})$	$0.283\,\tau^{1D}$
10	$0.874\exp(-2.042\,T^{1D})$	$0.274\,\tau^{1D}$
15	$0.857\exp(-2.169\,T^{1D})$	$0.249\,\tau^{1D}$
20	$0.846\exp(-2.238\,T^{1D})$	$0.236\,\tau^{1D}$
30	$0.835\exp(-2.311\,T^{1D})$	$0.223\,\tau^{1D}$
50	$0.826\exp(-2.372\,T^{1D})$	$0.212\,\tau^{1D}$
100	$0.818\exp(-2.412\,T^{1D})$	$0.205\,\tau^{1D}$
∞	$0.811\exp(-2.470\,T^{1D})$	$0.197\,\tau^{1D}$

Appendix A.4. Approximation of the solution for $\mathcal{B}^{1D} \sim 1$

As neither the limiting cases are likely to describe leaves operating under normal conditions, and (A.17) is not easily implemented by many plant physiologists, an approximate solution relating time and potential when $\mathcal{B}^{1D} \sim 1$ is desirable. For any observed half time, each value of $\mathcal{B}^{1D}$ provides a unique combination of particular values of h and k_ℓ^{1D}. Bringing together the definitions of the 1D Biot number ($\mathcal{B}^{1D} = hL/k_\ell^{1D}$), the characteristic time ($\tau^{1D} = c_\ell^{1D}L^2/k_\ell^{1D}$) and the expression for the halftime ($t_{1/2} = T^{1D}_{1/2} \cdot \tau^{1D}$),

$$\tau^{1D} = \frac{c_\ell^{1D} L}{h}\mathcal{B}^{1D} \quad \rightarrow \quad t_{1/2} = \frac{c_\ell^{1D} L}{h}\left(\mathcal{B}^{1D} \cdot T^{1D}_{1/2}\right). \quad \text{(A.19)}$$

Regression analysis of the data in Table A.1 shows that the parenthetical term on the RHS of (A.19), the Biot number times the non dimensional halftime, is in turn well approximated by the simple linear function $0.2\mathcal{B}^{1D} + 0.73$ ($r^2 = 0.999$). Using the definition of the Biot number, we then find

$$t_{1/2} = 0.2\frac{c_\ell^{1D} L^2}{k_\ell^{1D}} + 0.73\frac{c_\ell^{1D} L}{h}. \quad \text{(A.20)}$$

As the range of $\mathcal{B}^{1D}$ in the regression is weighted towards values less than one, the second coefficient approaches the $T^{1D}_{1/2}$ of the solution in the $\mathcal{B}^{1D} \ll 1$ limit, whereas as the values of $\mathcal{B}^{1D}$ are weighted towards those larger than one, the first coefficient approaches the $T^{1D}_{1/2}$ of the solution in the limit $\mathcal{B}^{1D} \gg 1$. A more general approximation for the full range of $\mathcal{B}^{1D}$ is then given by,

$$t_{1/2} = 0.197\frac{c_\ell^{1D} L^2}{k_\ell^{1D}} + 0.693\frac{c_\ell^{1D} L}{h}. \quad \text{(A.21)}$$

This result suggests that we may approximate the halftime for a leaf characterized by any Biot number as the sum of the two limiting solutions, or,

$$t(\Psi) = T^{1D}(\mathcal{B}^{1D} \gg 1, \Psi)\tau^{1D} + T^{1D}(\mathcal{B}^{1D} \ll 1, \Psi)\frac{\tau^{1D}}{\mathcal{B}^{1D}}, \quad \text{(A.22)}$$

where the non dimensional times on the RHS are found by inverting equations (A.5) or (27) and (28) respectively. Equation (30) can be interpreted as saying that the hydration time for a leaf with any Biot number is just the time for permeation through the tissue, neglecting vascular resistance, plus a contribution from flow through the vasculature that decays to zero as the Biot number becomes large.

References

Armacost, R., 1944. The structure and function of the border parenchyma and vein-ribs of certain dicotyledon leaves. Proceedings of the Iowa Academy of Science 51, 157–169.

Boyce, C.K., Brodribb, T.J., Feild, T.S., Zwieniecki, M.A., 2009. Angiosperm leaf vein evolution was physiologically and environmentally transformative. Proceedings of the Royal Society B 276, 1771–1776.

Boyer, J.S., 1968. Relationship of leaf water potential to leaf growth. Plant Physiology 43, 1056–1062.

Boyer, J.S., 1969. Free-energy transfer in plants. Science 163, 1219–1220.

Boyer, J.S., 1985. Water transport. Annual Review of Plant Physiology 36, 473–516.

Boyer, J.S., 1995. Measuring the Water Status of Plants and Soils. Academic Press, San Diego, CA.

Bridgman, P., 1922. Dimensional Analysis. Yale University Press, New Haven, CT, USA.

Brodribb, T.J., Feild, T.S., Jordan, G.J., 2007. Leaf maximum photosynthetic rate and venation are linked by hydraulics. Plant Physiology 144, 1890–1898.

Brodribb, T.J., Feild, T.S., Sack, L., 2010. Viewing leaf structure and evolution from a hydraulic perspective. Functional Plant Biology 37, 488–498.

Brodribb, T.J., Holbrook, N.M., 2004. Diurnal depression of leaf hydraulic conductance in a tropical tree species. Plant, Cell and Environment 27, 820–827.

Brodribb, T.J., Holbrook, N.M., 2006. Declining hydraulic efficiency as transpiring leaves dessicate: two types of responses. Plant, Cell and Environment 29, 2205–2215.

Carslaw, H., Jaeger, J., 1959. Conduction of Heat in Solids. Oxford University Press, New York, NY.

Cochard, H., Nardini, A., Coll, L., 2004. Hydraulic architecture of leaf blades: where is the main resistance? Plant, Cell and Environment 27, 1257–1267.
Crank, J., 1957. The Mathematics of Diffusion. Oxford University Press, New York, NY.
Deen, W.M., 1998. Analysis of Transport Phenomena. Oxford University Press, New York, NY, USA.
Dengler, N., MacKay, L., 1975. The leaf anatomy of beech, *Fagus grandifolia*. Canadian Journal of Botany 53, 2202–2211.
Dudukovic, M., Mills, P., 1985. A correction factor for mass transfer coefficients for transport to partially impenetrable or nonadsorbing surfaces. American Institute of Chemical Engineers 31, 491–494.
Foster, J., Smith, W., 1986. Influence of stomatal distribution on transpiration in low wind environments. Plant, Cell and Environment 9, 751–759.
Horowitz, P., Hill, W., 1989. The Art of Electronics. Cambridge University Press, Cambridge, UK. 2nd edition.
Knipfer, T., Das, D., Steudle, E., 2007. During measurements of root hydraulics with pressure probes, the contribution of unstirred layers is minimized in the pressure relaxation mode: comparison with pressure clamp and high-pressure flow meter. Plant, Cell and Environment 30, 845–860.
Lienhard IV, J., Lienhard V, J., 2006. A Heat Transfer Textbook. Phlogiston Press, Cambridge, MA, USA.
Maier-Maercker, U., 1983. The role of peristomatal transpiration in the mechanism of stomatal movement. Plant, Cell and Environment 6, 369–380.
Meidner, H., 1975. Water supply, evaporation, and vapour diffusion in leaves. Journal of Experimental Botany 26, 666–673.
Mott, K.A., Peak, D., 2011. A new, vapour-phase mechanism for stomatal responses to humidity and temperature. Plant, Cell and Environment 34, 162–178.
Noblin, X., Mahadevan, L., Coomaraswamy, I.A., Weitz, D.A., Holbrook, N.M., Zwieniecki, M.A., 2008. Optimal vein density in artificial and real leaves. Proceedings of the National Academy of Sciences of the United States of America 105, 9140–9144.
Philip, J., 1958a. Osmosis and diffusion in tissue: Half-times and internal gradients. Plant Physiology 33, 275–278.
Philip, J., 1958b. The osmotic cell, solute diffusibility, and the plant water economy. Plant Physiology 33, 264–271.
Pieruschka, R., Huber, G., Berry, J., 2010. Control of transpiration by radiation. Proceedings of the National Academy of Sciences of the United States of America 107, 13372–13377.
Rockwell, F.E., 2010. Leaf water transport. Ph.D. thesis. Harvard University. Cambridge, MA, USA.
Rockwell, F.E., Holbrook, N.M., Stroock, A., 2014. Leaf hydraulics I: Scaling transport properties from single cells to tissues. Journal of Theoretical Biology 340, 251–266.
Rockwell, F.E., Holbrook, N.M., Zwieniecki, M.A., 2011. Hydraulic conductivity of red oak (*Quercus rubra* L.) leaf tissue does not respond to light. Plant, Cell and Environment 34, 565–579.
Russin, W., Evert, R., 1984. Studies on the leaf of *Populus deltoides* (Salicaceae): morphology and anatomy. American Journal of Botany 71, 1398–1415.
Sack, L., Melcher, P.J., Zwieniecki, M.A., Holbrook, N.M., 2002. The hydraulic conductance of the angiosperm leaf lamina: a comparison of three measurement methods. Journal of Experimental Botany 53, 2177–2184.
Sack, L., Streeter, C., Holbrook, N.M., 2004. Hydraulic analysis of water flow through leaves of sugar maple and red oak. Plant Physiology 134, 1824–1833.
Salleo, S., Raimondo, F., Trifilo, P., Nardini, A., 2003. Axial-to-radial water permeability of leaf major veins: a possible determinant of the impact of vein embolism on leaf hydraulics? Plant, Cell and Environment 26, 1749–1758.
Scoffoni, C., Pou, A., Aasamaa, K., Sack, L., 2008. The rapid light response of leaf hydraulic conductance: new evidence from two experimental methods. Plant, Cell and Environment 31, 1803–1812.
Tyree, M.T., Cheung, Y., 1977. Resistance to water-flow in *Fagus grandifolia* leaves. Canadian Journal of Botany 55, 2591–2599.
Wylie, R.B., 1939. Relations between tissue organization and vein distribution in dicotyledon leaves. American Journal of Botany 26, 219–225.
Ye, Q., Holbrook, N.M., Zwieniecki, M.A., 2008. Cell-to-cell pathway dominates xylem-epidermis hydraulic connection in *Tradescantia fluminensis* (Vell. Conc.) leaves. Planta 227, 1311–1319.
Zwieniecki, M.A., Brodribb, T.J., Holbrook, N.M., 2007. Hydraulic design of leaves: insights from rehydration kinetics. Plant, Cell and Environment 30, 910–921.